Experimental Study of DKPP-βT Polymeric Thin Film Transistor

Experimental Study of DKPP-βT Polymeric Thin Film Transistor

BY

Cong Feng, B.Eng.

A Thesis

SUBMITTED TO THE DEPARTMENT OF ELECTRICAL & COMPUTER ENGINEERING

AND THE SCHOOL OF GRADUATE STUDIES

OF MCMASTER UNIVERSITY

IN PARTIAL FUILFILMENT OF THE REQUIREMENTS

FOR THE DEGREE OF

MASTER OF APPLIED SCIENCE

Master of Applied Science (2012) McMaster University

(Electrical & Computer Engineering) Hamilton, Ontario, Canada

TITLE: Experimental Study of DKPP-βT Polymeric Thin Film Transistor

AUTHOR: Cong Feng

B.Eng, (Information Engineering)

Southeast University, Nanjing, China

SUPERVISOR: Professor M. J. Deen

NUMBER OF PAGES: LXXXI

Dedicated to my mother and father

Abstract

In the last 30 years, the possibility of using polymeric thin film transistors (PTFTs) in flexible display, sensors, radio-frequency identification tag and the potential of using printing or low-cost reel-to-reel fabrication techniques has stimulated much research and technology development in these devices. However, the utilization of PTFTs needs better understanding of the organic semiconductor material's properties and their physical and chemical mechanisms. In addition, the PTFTs show poor stability compared to the crystalline transistors. The PTFTs can have significant variations of threshold voltage, mobility, on/off ratio even when deposited using the same conditions on the same substrate. Therefore, better understanding of the PTFTs' physical and chemical properties and the improvement of the characterization techniques are needed.

The design and fabrication of the novel polymeric semiconductor, diketopyrrolopyrrole β-unsubstituted quaterthiophene (DKPP-βT) based bottom-gated top-contact PTFT and microfluidics PTFT are introduced in this thesis. The microfluidic PTFT consists of polydimethylsiloxane (PDMS) microchannel which guides liquids flowing over the top of the semiconductor channel.

From consecutive electrical measurements, it was found that the threshold voltage (V_T) follows a logarithmic law function of the time. Illuminating the PTFTs results in shifts of the initial value of the threshold voltage linearly towards more positive value. The mobility is unaffected by time or by illumination. However, the off current increased

proportionally with light. Also, the contact resistance extracted by the parameter compensated transmission line model (TLM) method is ohmic and gate bias independent for high gate biases.

The novel microfluidic PTFT enables the study of the sensing property of the DKPP-βT PTFT of liquid analytes. The threshold voltage evolution in the deionized (DI) water measurements also follows logarithmic function of the time with a slightly steeper slope than in air. The mobility only slightly decreases initially on exposure to DI water. The off current in DI water measurements decrease compared with air measurements. In acid solution measurements, the threshold voltage remains stable and the mobility slightly increased, compared with measurements in water. Additionally, the subthreshold slope and off current in both acid solution and salt water measurements show similar results to the DI water measurements. While the base solution damages the device immediately. The stable performance of DKPP-βT PTFTs with DI water and low-concentration salt water in the microchannel makes it a promising biosensor.

Acknowledgements

Firstly, I would like to express my sincere gratitude to my supervisor Dr. Jamal Deen for giving me the opportunity and trusting me to work in this project. I am deeply grateful for his excellent guidance and strong support for my entire project. I feel fortunate to work with such an extraordinary professor.

I would like to thank Dr. Ravi Selvaganapathy for his invaluable comments and guidance that help me overcome several difficulties in research. I also would like to express my appreciation to Dr. Yiliang Wu for his constructive suggestions and discussion on the fabrication techniques and measurement results.

Next, I would like to thank Dr. Marinov for his critical comments and suggestions on the experimental results and data analysis. I am grateful for Tianyi Guo for his practical suggestions and patient discussions. Also, many thanks to Zhiyun Li for always supporting me.

I would like to express my thanks for the support from CEDT and ECE staff Doris Stevanovic, Zhilin Peng, and Terry Greenlay, Joe Verhaeghe. Thanks to all my friends Fangfang, Derek, Hani, Wen, Pouya, Bo, Leo, Siawash, Peter, Chad, Cam and Yujie for their help in my research and providing me a good environment.

Last but not the least, I would like to thank my family members who always support me. I am in debt forever for their continuous support and love.

Abbreviations

PTFT	Polymeric thin film transistor
MOSFET	Metal-oxide-semiconductor field effect transistor
HOMO	Highest occupied molecular orbital
LOMO	Lowest unoccupied molecular orbital
MTR	Multiple trapping and thermal release model
VRH	Variable range hopping
TLM	Transmission line model
P3HT	Poly (3-hexylthiophene)
P3OT	Poly (3-octylthiophene)
SAM	Self assembled monolayer
OTS	Octyltrichlorosilane
DKPP-βT	Diketopyrrolopyrrole β-unsubstituted quaterthiophene
PDMS	Polydimethylsiloxane
HF	Hydrofluoric acid
IPA	Isopropanol
CEDT	Centre for Emerging Device Technologies
DDFTTF	5, 5'-bis-(7-dodecyl-9H-fluoren-2-yl)-2,2'-bithiophene

Contents

List of Figures

Chapter 1 Motivation and Organization

1.1Motivation

In the last 30 years, much research efforts have been dedicated to studying polymeric thin film transistor (PTFT) since it has the potential of printability using reel-to-reel large volume fabrication techniques to reduce the manufacturing cost [1].

Many polymers are being used as insulators. In fact, the electrical conductivity of polymer was regarded as non-ideal behavior not too long ago [1]. In 1862, Henry Letheby obtained conductive polyaniline by oxidizing aniline in sulfuric acid solution [2]. In 1963, McNeill et al. reported high conductivity (σ) polymer (1 S/cm) [3, 4]. The research of conducting polymer boomed after the discovery that polyacetylene $(CH)_x$ can be doped by halogen, and by 1977, the conductivity had increased up to eleven orders of magnitude [5-7]. Later, three scientists, Alan J. Heeger, Alan G. MacDiarmid and Hideki Shirakawa, jointly won the Nobel Prize in Chemistry in 2000 "for the discovery and development of conductive polymers" [8]. In 1987, the first polymeric thin film transistor was obtained by Koezuka et al using polythiophene as the semiconductor material [9].

Nowadays, organic light-emitting diodes (OLEDs) have been commercialized for light weight and wider viewing angles display by companies such as Samsung [10], Philips, Sony [11]. Figure 1-1 shows a conceptual full color organic flexible display product that can be rolled up into a “pen” when it is not used [12].

Figure 1-1 Conceptual diagram for the full color organic flexible display [12]

The potential of low cost fabrication and diversity of organic semiconductors make organic thin film transistor (OTFT) promising as high sensitivity, disposable and inexpensive biological and chemical sensors [13]. The OTFT sensing property of gases, such as oxygen [14],[15],[16], water vapor [16],[17],[18],[19], alcohols [20],[21], NO_2 [22], nitrogen [16] have been studied. In [23], a pentacene OTFT DNA sensor was fabricated. That sensor was based on the mechanism that phosphate groups at DNA backbone attract electrons and shift the OTFT threshold voltage towards positive value. The possibility of using PTFTs in flexible display, sensors as well as RFID tag boosts the research of PTFTs.

The motivation of this work is as following. (1) The utilization of PTFTs needs improved characterization techniques and better understanding of the organic semiconductor material's properties. Moreover, a more complete understanding of many physical and chemical mechanisms of PTFT is required. (2) The PTFTs show poor stability compared

to the crystalline transistors. The polymeric thin film transistors can have significant variations of current [24], threshold voltage [25], mobility, on/off ratio even when deposited using the same conditions on the same substrate. The PTFTs also show instabilities during operation, both in inert environment or when encapsulated. The instabilities, such as threshold voltage shift and variations of the current are commonly observed. Therefore, better understanding of the PTFTs' physical and chemical properties and the improvement of the characterization techniques are needed. For instance, normalizing to the starting point value, the PTFTs can have similar behaviors although the devices on the same substrate were with large differences in the currents at the starting point [26].

1.2 Organization of the thesis

In chapter two, the typical solution deposition method, organic semiconductor and device configuration of polymeric thin film transistor are discussed. The generic DC model and parameter extraction techniques are introduced and the contact resistance obtained by transmission line model method is described. The poor environmental and operational stability of PTFT are discussed.

In chapter three, the fabrication techniques of PTFT and microfluidic PTFT are introduced. Also, the selected material, including self assembled monolayer, semiconductor, metal and PDMS used in the fabrication process, are described.

In chapter four, the experimental setup and design methods in this work are introduced. The behavior of PTFT and microfluidic PTFT under different experimental conditions are studied. The data analysis methods are based on the techniques introduced in chapter 2.

In chapter five, a summary of the PTFT's parameter evolution and microfluidic the PTFT under different measurement conditions is presented.

In the last chapter, the contributions of this work are provided. Additionally, possible utilization of the microfluidic PTFT as biosensor and the improvement to some identified problems are introduced.

Chapter 2 Introduction to Polymeric Thin Film Transistors (PTFTs)

For decades, the possibility of large volume reel-to-reel fabrication of PTFTs without using the expensive vacuum fabrication techniques has boosted the research in organic transistors. In this chapter, the PTFT configuration, solution deposition method, characterization methods and operational stability are discussed.

Figure 2-1 Commercial reel-to-reel printed by Poly IC [27]

2.1 Fabrication, structure, and material of PTFTs

2.1.1 Solution deposition method of PTFTs

In early 1990s, the fully printed PTFT was realized. Francis Garnie et al. screen printed PTFT, where a blade pushes the ink go through a steel screen mask depositing onto the substrate, as shown in figure 2-2(a) [28] . The screen printing technique is applicable to high speed and large volume manufacturing. However, the resolution of screen printing is around 35~100 μm [29] which is too large for practical electronics applications. Also, the high viscosity ink is needed in screen printing, which is also difficult to achieve in organic material [30]. The stamp printing (microcontact printing) method uses the

patterned elastomer stamp printing the ink onto the substrate, as shown in figure 2-2(b). Rogers et al. have demonstrated 2μm resolution by using the elastomer stamp for deposition of self assembled monolayer (SAM) which resists the etching of the pre-deposited metal layer [31]. The stamp printing also can be used in the large volume reel-to-reel manufacturing.

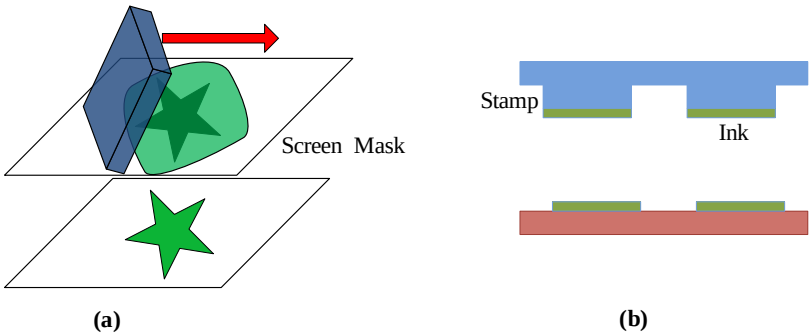

Figure 2-2 (a) Illustration of screen printing (b) Illustration of stamp printing

The inkjet printing technique is widely used in research on PTFTs [30]. The piezoelectric inkjet printing system injects the droplet through a pinhole to the designated spot on the substrate with high resolution (25μm for Dimatix Materials Printer DMP-2800 [32]). It allows the use of CAD software for designing patterns, controlling of the droplet velocity, volume, and distance between droplets. Compared with screen printing and the gravure printing, the inkjet printing gives higher resolution, but low throughput. A fiducial camera captures the printed patterns which assist in good controllability of the printing quality [32]. Therefore, the inkjet printing system with 16 or more nozzles is suitable for research. However, the low productivity does not satisfy the high volume and low cost manufacturing demanded in industry.

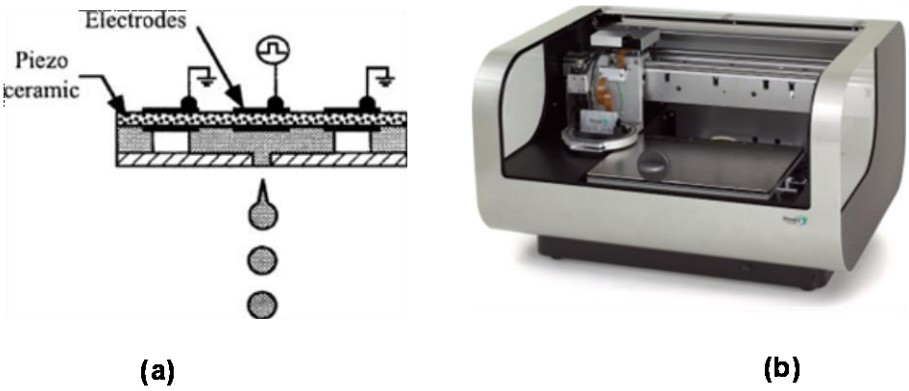

Figure 2-3 (a) Schematic of piezoelectric inkjet printing [33] (b) Dimatix Materials Printer DMP-2800 [32]

2.1.2 PTFTs structure

The typical test structures of polymeric thin film transistor including bottom-contacted bottom-gated PTFT, and top-contacted bottom-gated PTFT, top-contacted patterned-bottom-gated PTFT, are shown in figure 2-4.

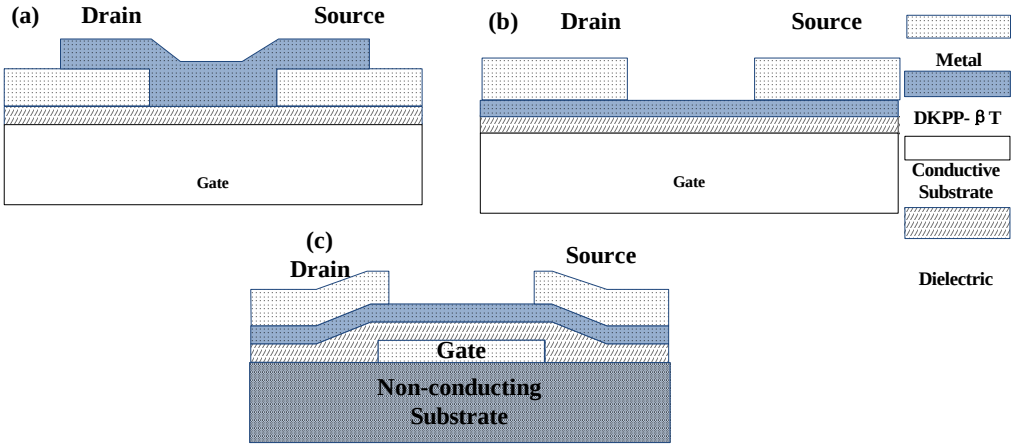

Figure 2-4 Schematic of PTFT structures (not to scale) (a) bottom-contacted bottom-gated PTFT, (b) top-contacted bottom-gated PTFT, (c) top-contacted patterned-bottom-gated PTFT

Similar to the metal-oxide-semiconductor field effect transistor (MOSFET), the PTFT has three terminals — drain, source and gate. The current between drain and source terminals is controlled by the gate terminal. By applying negative gate bias (p-type semiconductor), a very thin conduction channel can be accumulated within the active layer next to the surface of the insulator layer, as shown in figure 2-5.

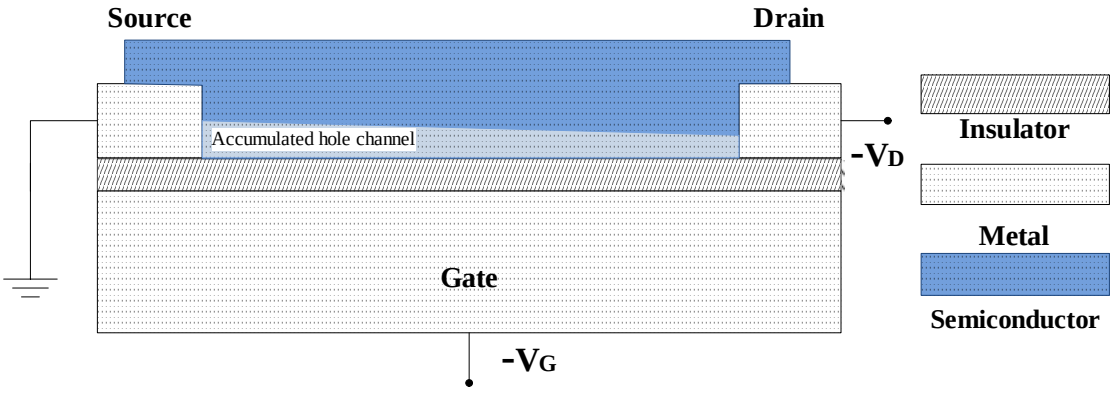

Figure 2-5 Accumulated hole channel formation in PTFTs at bias of $0>V_D>(V_G-V_T)$,$V_S=0$

All parts in bottom-contacted bottom-gated PTFT, except for the organic thin film layer, can be fabricated using traditional semiconductor fabrication techniques such as photolithography, vacuum evaporating and sputtering, which are accessible in most laboratories. However, the solution deposition of the active layer on the surfaces of metal electrode and dielectric layer simultaneously always results in non-uniformity of the film [34] due to the different properties of metal and dielectric. Consequently, the irregular film at the metal-dielectric interface, as shown in figure 2-6, results in the large contact resistance of PTFT.

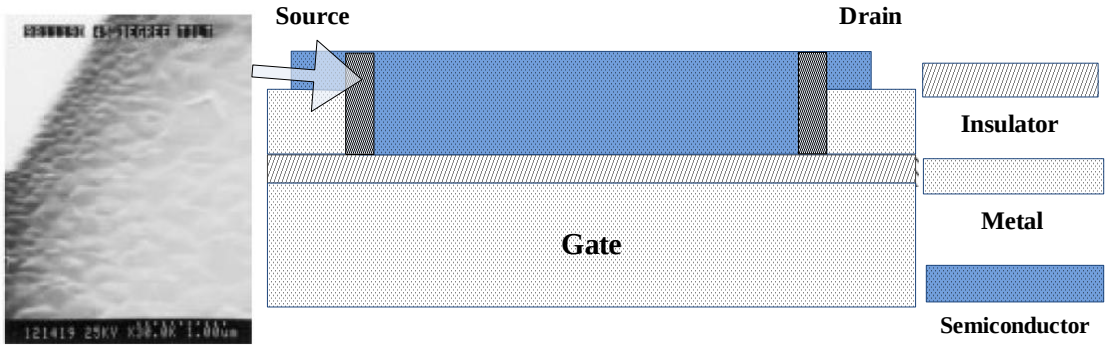

Figure 2-6 Nonuniform active layer film in the bottom contact PTFT configuration (a) Pentacene deposited on Au (up-left) and SiO_2 (down-right) [34] (b) Bottom-contacted bottom-gated PTFT with disordered thin film at contacts [35]

Bottom-gated top-contacted PTFT is routinely used to study the characteristics of new materials. Except for the active layer, all parts can be fabricated using standard semiconductor fabrication techniques. Different from the bottom contacted PTFTs, the organic semiconductor of top-contacted PTFT deposited on top of the insulator layer (for instance silicon dioxide) leads to a well ordered organic semiconductor thin film

formation. After that, the vacuum evaporation of the metal through a shadow mask avoids the damage of active layer in photolithography. The drain and source pads grow firmly on the top of organic semiconductor thin film with lower contact resistance. However, the poor resolution of the shadow mask results in large dimension devices.

In the non-patterned gate structures, the PTFTs cannot be individually controlled on the same substrate, because of the common gate. However, for circuits, the transistors should be controlled separately, and the patterned-bottom-gated PTFT can be used. The gate electrode is deposited first on the substrate and then the polymer dielectric is spin-coated or printed on the top. However, the polymeric dielectric has larger leakage compared with the thermally growth SiO_2 and the fabrication procedure is more complicated.

2.1.3 Organic semiconductor

The most of the conducting organic materials consist of π-bonding system, which means the molecules have double and single bonds, as shown in figure 2-7. Pentacene, PQT and P3HT are widely used organic materials in research [36].

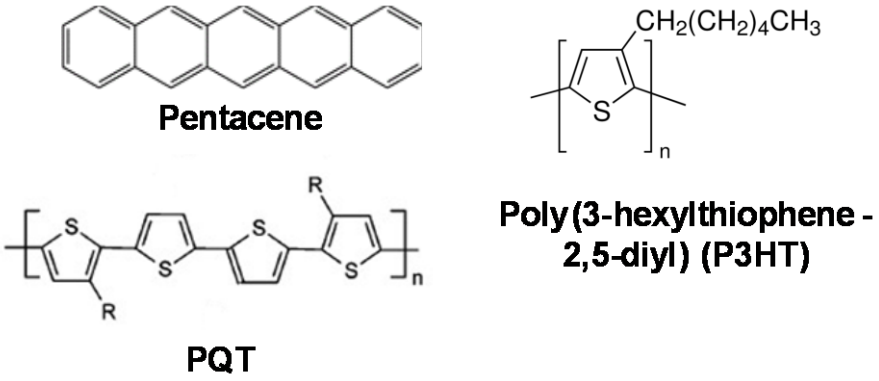

Figure 2-7 Chemical structure of typical organic semiconductor [36]

Take double bond in ethene as an example, shown in figure 2-8. Each carbon atom has three sp^2 hybridized orbitals and a p orbital, where two sp^2 hybridized orbitals form σ-bonds with two hydrogen atoms respectively. The σ-bond is the strongest covalent bond between atoms. The left sp^2 hybridized orbital forms the first bond, the σ-bond, in the double bond between two carbon atoms, where two sp^2 hybridized orbitals overlap and point to the two carbon atoms. The σ-bond draws the two carbon atoms close to each other and the left two p orbitals, which are perpendicular to the carbon-carbon plane, overlap and form a π-bond. The π-bond is the second bond in the double bond and allows the electrons move between the neighbor carbon atoms. Afterwards, the consecutive π-bond allows the electrons form a π-cloud where the electrons are delocalized and move across many atoms within a molecule [36].

Because the π-bond is out of plane of the carbon atoms, the π-cloud in the adjacent molecule can overlap and the electrons can move between nearby molecules. Therefore the well ordered molecules structure in the intermolecular electron movement, like the well ordered π-stacking lamellar structure, is very important in the charge transport in the organic semiconductor [36].

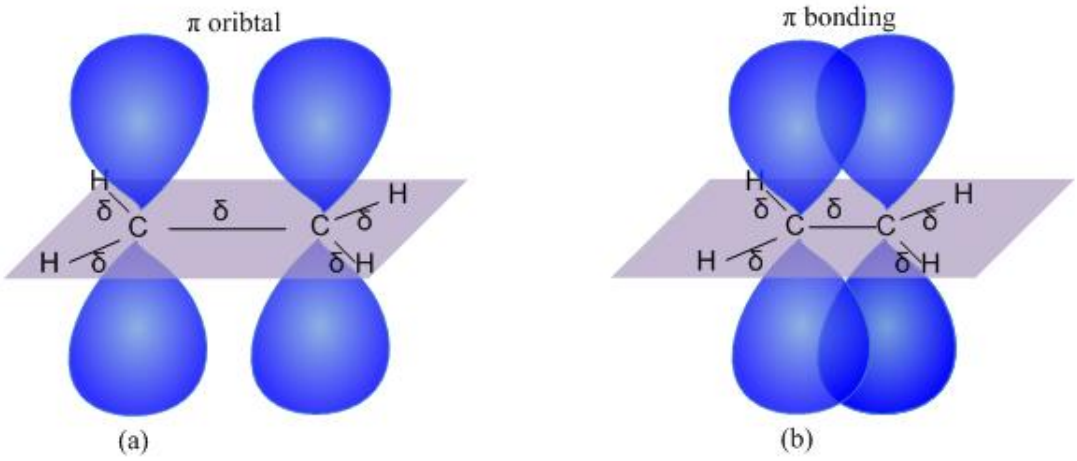

Figure 2-8 Orbital structure of Ethene. (a) The first bond in the double bond between two carbon atoms is the overlapping of sp^2 orbital formed σ-bond. (b) σ bond drags the two carbon atoms closer to each other and the two p orbital overlapping forms π-bond [37].

There are several theories explaining the charge transport in organic semiconductor. Assuming that the organic material is similar to semiconductors, then the band-like structure can be adopted from inorganic semiconductors. The σ -bond is much stronger than the π-bond, and the electrons in π orbitals split their energy levels into a band like energy distribution, where the band is narrower than the band in silicon. The highest occupied molecular orbital (HOMO) and the lowest unoccupied molecular orbital (LUMO) are analogous to the valence band and the conduction band, respectively. In the multiple trapping and thermal release (MTR) models, the assumptions are (1) the charge carriers are captured with a probability close to one once they reach traps; (2) the trapped charges are released by thermal excitation. The effective mobility μ_{eff} is proportional to the ratio of the free and trapped charges [36]. With application of gate bias, the difference between charge-occupied energy levels (traps) and the transport band edge is reduced,

which makes thermal excitation to release the localized in traps charges easier into the transport band, where the charge is mobile. Therefore the mobility increases with increasing gate bias [38].

In the variable range hopping (VRH) model, the organic material is assumed as semi-insulator, which means that the charge carriers are occupying localized states and hopping between the different states by some probability. The gate bias increases the occupation of the states (hole), thus, reduces the distance between the states, increases the hopping probability, and results in increased mobility as well. Interestingly, despite the different assumptions, the mobility derived from MTR and VRH has the same gate bias dependence finally [38].

Because of the exponential energy distribution of the density of states [25], the mobility is enhanced with the gate bias voltage V_G as a power-law function, that is, the mobility is proportional to the V_G on some exponent called mobility enhancement factor γ [38]. This gate bias enhancement of the mobility in PTFT (and other amorphous-material TFTs) is the main difference in comparison to the crystalline MOS transistor. In the latter, the mobility is constant or decreases with V_G, owing to unaltered or increased surface carrier scattering at the semiconductor-insulator interface.

2.2 Characteristics and extraction techniques for PTFTs

2.2.1 PTFTs characteristics

The PTFT has similar behavior with metal-oxide-semiconductor field effect transistor (MOSFET), as shown in figure 2-9.

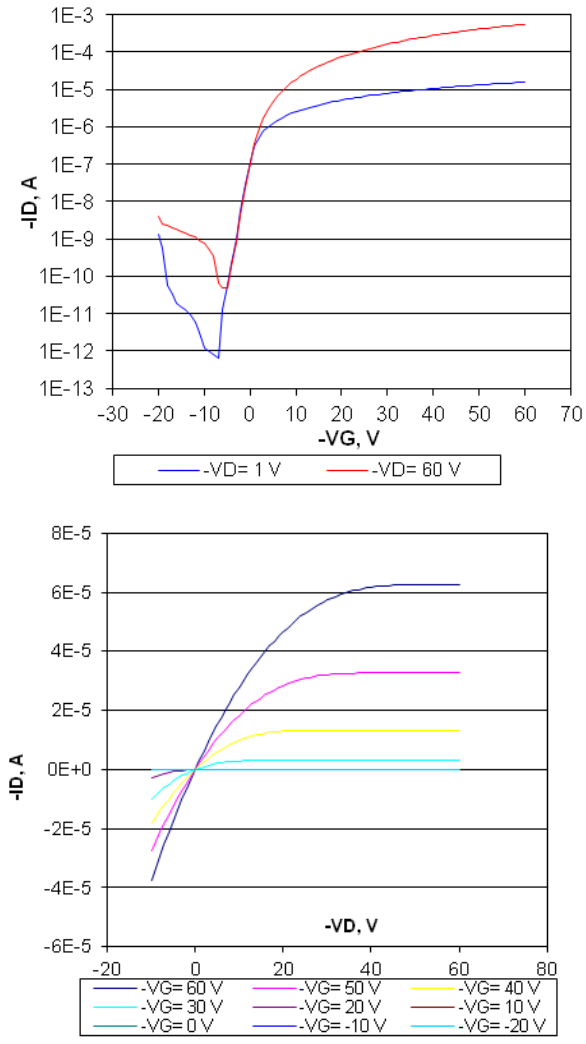

Figure 2-9 typical DKPP-βT top-contacted bottom-gated PTFT I-V characteristic with W/L=5000μm/90μm, (a) log I_D vs. V_G (b) I_D vs. V_D

The drain current I_D depends on the ratio of channel width W and length L. I_D is proportional to the unit area gate dielectric capacitance C_{OX} and increases with the terminals' bias voltage. Hence, the drain current can be approximately described using MOS model, given by

$$I_D = \frac{W}{L}\mu C_{OX}\begin{cases}(V_G - V_T)V_D\text{, in linear regime, when} V_D \ll (V_G - V_T)\\ \frac{1}{2}(V_G - V_T)^2\text{, in saturation regime, when } V_D > (V_G - V_T)\end{cases} \quad (2\text{-}1)$$

where μ is the charge carrier mobility, V_G and V_D are the gate and drain bias respectively, and V_T is the threshold voltage. However this simple model is not appropriate for PTFT, since the mobility μ has gate bias dependent and the contact resistance is not negligible at high gate biases.

2.2.2 Extraction techniques for transfer characteristic

The threshold voltage and mobility can be extracted from equation (2-1). In the linear regime $I_D = (V_G - V_T)V_D\, K \Longrightarrow K = (\text{slope of } I_D \text{ vs. } V_G)/V_D$,

$V_T = X - \text{intercept of } I_D \text{ vs. } V_G$. And in saturation regime $\sqrt{I_D} = (V_G - V_T)\sqrt{K/2}$,

$\Longrightarrow K = 2 \times (\text{slope of } \sqrt{I_{Dsat}} \text{ vs. } V_G)^2, V_T = X - \text{intercept of } \sqrt{I_D} \text{ vs. } V_G,$

where the transistor constant $K=(W/L)\mu C_{OX}$ is proportional to the slope, as shown in figure 2-10.

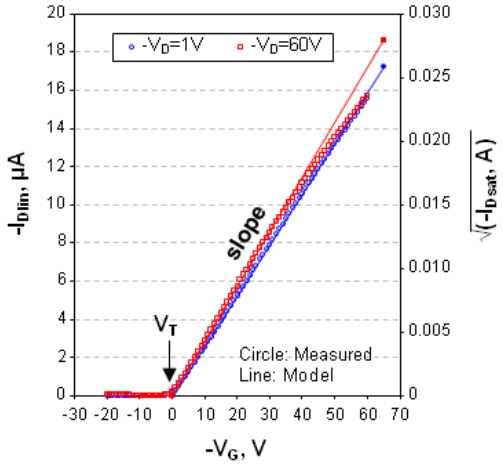

Figure 2-10 I_{Dlin} and $\sqrt{I_{Dsat}}$ vs. V_G

In the MOS model, the bias enhancement of mobility and the contact resistance R_C have been neglected, namely, assuming $I_D \times R_C = 0$ and mobility enhancement factor $\gamma = 0$. However, these assumptions are not accurate for PTFT, because the charge carrier mobility μ increases as the gate bias increases, as $\mu \propto (V_G - V_T)^{\gamma}$ [39],[40].

In the generic DC model [39], the drain current is given by

$$I_D = \frac{W}{L}\mu_o C_{OX}\frac{(V_G - V_T - V_S)^{(\gamma+2)} - (V_G - V_T - V_D)^{(\gamma+2)}}{\gamma+2} \quad (2\text{-}2)$$

where $\mu = \mu_o(V_G - V_T)^{\gamma}$ when the potential at source terminal $V_S = 0$. μ_o has different unit from the mobility μ, and is defined as $\mu_o = \mu_{oo}/(V_\gamma)^{\gamma}$, where μ_{oo} is the low-field mobility when $(V_{G\gamma} - V_T) = V_\gamma = 1V$, hence, μ_o has the same value with the low field mobility μ_{oo}. V_D is the channel potential of drain side in linear regime, or ~$(V_G - V_T)$ in the saturation regime. V_S is the channel potential at source side [39].

2.2.2.1 The $H_{VG}(V_G)$ function extraction technique

The $H_{VG}(V_G)$ function is used to extract the threshold voltage V_T and mobility enhancement factor γ first for the linear regime [41], and then extended for both of the linear and saturation regimes [42].

The H_{VG} function is given by

$$H_{VG}(V_G > V_T) = \frac{\int_{\sim V_T}^{V_G > V_T} I_D(V_G) dV_G}{I_D(V_G > V_T)} \approx \begin{cases} \frac{(V_G - V_T)}{2 + \gamma}, & \text{in linear regime, when} V_D \ll (V_G - V_T) \\ \frac{(V_G - V_T)}{3 + \gamma}, & \text{in saturation regime, when } V_D > (V_G - V_T) \end{cases} \quad (2-3)$$

From the equation, the mobility enhancement factor γ and threshold voltage V_T can be extracted from the slope and the x-intercept of H_{VG} vs.V_G, as shown in figure 2-11. The benefit of this method is that W, L, μ_o and C_{OX} are canceled, and only V_T and γ remain. However, to make this extraction technique works, the PTFT should operate well in linear or saturation regimes, the contact resistance should be negligible. However, the assumptions are not precise for OTFT at high V_G.

In the linear regime at high V_G, the contact resistance reduces the mobility enhancement factor γ, which increases the H_{VG} slope. In the saturation regime with fixed V_D, the growing V_G leads the device to departure from saturation, making a transition to the linear

regime, resulting in increase of the slope of the H_{VG} from $\frac{1}{3+\gamma}$ to $\frac{1}{2+\gamma}$, as seen in the figure 2-11.

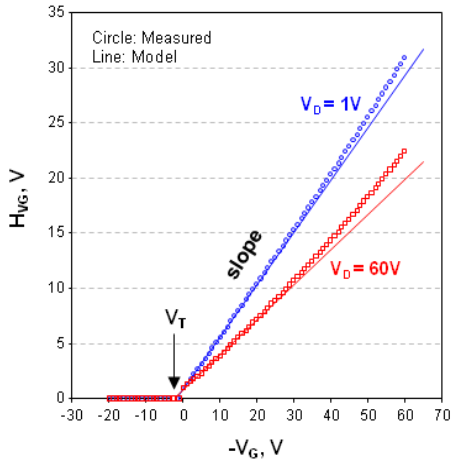

Figure 2-11 H_{VG} vs. V_G

2.2.2.2 Y-function extraction technique

The Y-function method was first developed for the gate bias degradation of mobility of MOSFET [43]. Then it was adapted for PTFT in linear regime with significant contact resistance, because the Y-function compensate for the contact resistance [44].

The Y-function method is used to extract the threshold voltage V_T and transistor constant $K_0 = (W/L)\mu_0 C_{OX}$. The assumptions are as follows, (1) the source and drain contact resistance are equal, $R = R_S = R_D = 1/2R_C$; (2) the PTFTs operate well in the linear regime, $(V_G - V_T) \gg V_D > I_D \times R_C$; (3) the mobility enhancement factor γ is small, $0 \leq \gamma < 1$ (typical values are between 0.3 and 0.6 for PTFT at room temperature).

Starting from the generic DC model of equation (2-2) in linear regime, the equation becomes

$$I_D \approx K_0(V_G - V_T - V_S)^{1+\gamma}(V_D - V_S)$$
$$\approx K(V_G - V_T - I_D R)^{1+\gamma}(V_D - 2I_D R) \quad (2-4)$$

The Y-function defined as the ratio of I_D and $\sqrt{g_m V_D}$, where g_m is the transconductance equals to $\frac{\partial I_D}{\partial V_G}$. The first two terms in Taylor series, $(1-x)^n \approx 1 - nx$, $1 - x \approx \frac{1}{(1+x)}$ when $|x| \approx 0$, are used in algebraic transformation. Then, the Y function is obtained as

$$Y_{VG} = \frac{I_D}{\sqrt{g_m V_D}} = \frac{\sqrt{K_0}}{\sqrt{1+\gamma}}(V_G - V_T)^{1+\gamma/2} \quad (2-5)$$

In equation (2-5), R is absent, hence, Y_{VG} function compensates for the contact resistance R_C. However, Y_{VG} vs. V_G is a power law function, as shown in equation (2-5). When $\gamma > 0$, the non-linearity leads to inaccuracy when estimating the threshold voltage V_T and the transistor constant K from linear regression. The slope in the power law function varies, and choosing different ranges for the linear regression, the slope and the intercept obtained from the linear fitting change. Figure 2-12 shows that the Y_{VG} is quasi-linear at low gate bias and bend up at high gate bias, which is due to the power law function $(V_G - V_T)^{1+\gamma/2}$ with $\gamma > 0$.

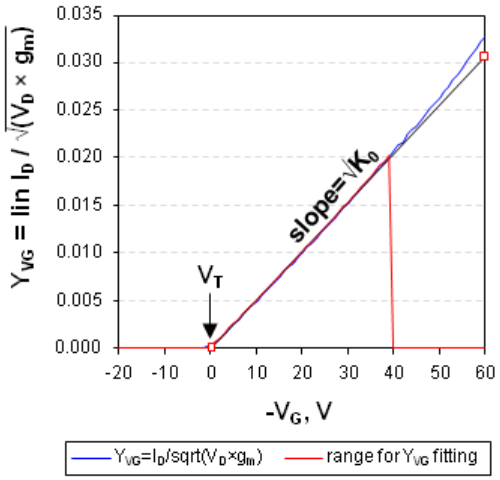

Figure 2-12 Y_{VG} vs. $-V_G$

From assumption (3), $\gamma < 0.6 < 1$, the terms in equation (2-5) are expanded using Taylor series.

$$\sqrt{1+\gamma} \approx 1+\frac{\gamma}{2}, \qquad \text{with small max error} \leq \frac{\gamma^2}{4} = \frac{0.6^2}{4} = 0.09 \qquad (2-6)$$

Expanding the $(V_G - V_T)^{1+\gamma/2}$ around $V_{G0} > V_T$ within the fitted range in figure 2-12, $(V_G - V_T)^{1+\gamma/2}$ becomes

$$(V_G - V_T)^{1+\gamma/2} \approx (V_{G0} - V_T)^{1+\gamma/2} + \left(1+\frac{\gamma}{2}\right)(V_{G0} - V_T)^{\frac{\gamma}{2}}(V_G - V_{G0})$$

$$\approx (V_{G0} - V_{TE})^{\gamma/2}\left(1+\frac{\gamma}{2}\right)^{1+\frac{\gamma}{2}}(V_G - V_{TE}) \qquad (2-7)$$

The estimated threshold voltage V_{TE} from the linearized power law function around V_{G0} is

$$V_{TE} = \frac{V_T + (\gamma/2)V_{G0}}{1+\gamma/2} \Rightarrow V_T = V_{TE} - \frac{\gamma}{2}(V_{G0} - V_{TE}) \qquad (2-8)$$

where the actual threshold voltage V_T is overestimated by $\gamma/2(V_{G0} - V_{TE})$. Note that lager the mobility enhancement factor γ and the selected V_{G0} result in the bigger V_T overestimation. The linear expansion equations (2-6) and (2-7) replace the power law function in equation (2-5), given by

$$Y_{VG} = \frac{I_D}{\sqrt{g_m V_D}} = \sqrt{K_0(V_{G0} - V_{TE})^{\gamma}(1 + \gamma/2)^{\gamma}} \times (V_G - V_{TE}) \qquad (2-9)$$

where the transistor constant K_E is

$$K_E = K_0(V_{G0} - V_{TE})^{\gamma}\left(1 + \frac{\gamma}{2}\right)^{\gamma}$$

$$\approx K_0(V_{G0} - V_{TE})^{\gamma}\left(1 + \frac{\gamma^2}{2}\right) \leq K_0(V_{G0} - V_{TE})^{\gamma} \times 1.2, \text{if } \gamma < 0.6 \qquad (2-10)$$

the transistor constant K_0 is overestimated by $(V_{G0} - V_{TE})^{\gamma} \times 1.2$.

In summary, the Y_{VG} function compensates for the contact resistance R_C, but overestimates threshold voltage V_T and transistor constant K_0 when mobility enhancement factor $\gamma > 0$. The high γ results in the bigger overestimations. Furthermore, the overestimation increases in the linear regression of Y_{VG} at high gate bias voltage. Therefore, Y_{VG} should be fitted at low gate bias voltage, as shown in figure 2-12.

2.2.2.3 The contact resistance R_c extracted from transfer curve

The contact resistance R_C extracted from transfer curve in the saturation regime is proposed here. First, we do not consider γ, and the drain current is given as

$$\frac{2I_D}{K} = (V_G - V_T - V_S - V_C)^2 = (V_{GTS} - V_C)^2 \qquad (2-11)$$

assuming that $R_C = R_S \approx$ constant, $K = \frac{W}{L}\mu C_{OX} =$ constant x . Then, taking the partial derivative of equation (2-11) gives

$$\frac{\partial \frac{2I_D}{K}}{\partial I_D} = \frac{2}{K} = 2(V_{GTS} - V_C)\left(\frac{\partial V_{GTS}}{\partial I_D} - R_C\right) = 2(V_{GTS} - V_C)(\frac{1}{g_m} - R_C)$$

Replacing $\sqrt{\frac{2I_D}{K}} = (V_{GTS} - V_C)$ in the equation above, we get

$$\frac{1}{g_m} = \sqrt{\frac{1}{2K}} \times \frac{1}{\sqrt{I_D}} + R_C \qquad (2-12)$$

Since the transconductance g_m and drain current I_D can be obtained from the experiments, as shown in figure 2-13, $\frac{1}{g_m}$ vs. $\frac{1}{\sqrt{I_D}}$ is plotted. The contact resistance R_C and transistor constant K can be found from the intercept and slope, respectively, as depicted in the plot figure 2-13.

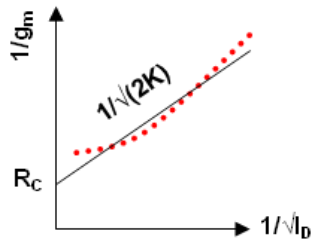

Figure 2-13 1/ g_m vs. 1/$\sqrt{I_D}$

2.2.2.4 Subthreshold slope extraction technique

The TFT compact model also can describe the subthreshold regime of operation of the PTFT, when $V_G < V_T$. In equation (2-2), and with $V = V_D$ or $V = V_S$ in the term $(V_G - V_T - V)$, one can use the interpolation with effective voltage overdrive defined as [39]

$$V_{EODRS} = V_{SS} \ln\left[1 + \exp\left(\frac{V_G - V_T - V_S}{V_{SS}}\right)\right]$$

$$V_{EODRD} = V_{SS} \ln\left[1 + \exp\left(\frac{V_G - V_T - V_D}{V_{SS}}\right)\right] \qquad (2-13)$$

where in the experiments $V_S = 0V$, $V_D = 1V,\ 60V$ for the linear and saturation regimes respectively, V_{SS} is the subthreshold slope parameter (in the unit of V per neper of drain current), and equation (2-2) becomes

$$I_D = K_0 \frac{V_{EODRS}^{2+\gamma} - V_{EODRD}^{2+\gamma}}{2+\gamma} + I_{Doff} \qquad (2-15)$$

where the transistor constant K_0 equals to $(\frac{w}{L}\mu_o C_{OX})$ and I_{Doff} is the leakage current, when the PTFT is off at very low gate bias, $V_G \ll V_T - V_{SS}$. The model fitting (line) to the experimental data (with small circles) is shown in Fig. 2-14.

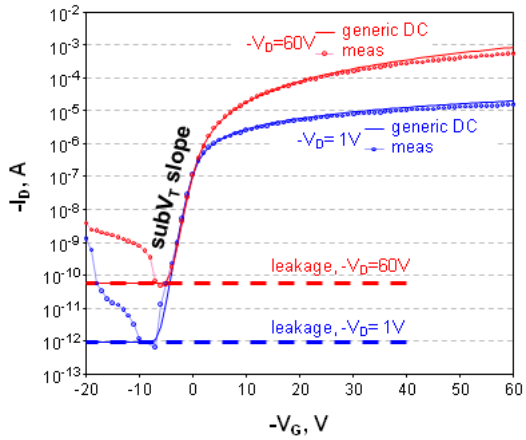

Figure 2-14 Transfer characteristic with model fitted in the subthreshold regime

The fitting neglects the contact resistance, assuming that $(V_G - V_T) \gg I_D \times R_C$. Therefore, drain current has been overestimated at high $(V_G - V_T)$. Leakage current is the mean value for the currents which are less than three times of the minimum drain current. The values of V_T, K_0, γ and V_{SS} are first adopted from the other extraction techniques (H_{VG}, Y_{VG} etc.) above, and then the values are varied until good fitting is achieved. By the variation of the parameter values, one compared the $\frac{\partial \ln (I_D)}{\partial V_G}$ slope of the measured and the modeling drain current within subthreshold regime, for instance V_G below $(V_T - 5V)$ and I_D more than 300× leakage current. The value of V_T and γ are varied until the standard deviation of the slope difference less than 0.001.

2.2.3 Extraction techniques for output characteristic

2.2.3.1 Saturation $\sqrt{I_D}$ vs. V_G extraction technique

The purpose of this method is to extract the threshold voltage and transistor constant $K = \frac{W}{L}\mu C_{OX}$ using the transfer characteristic of the PTFT. Assume that $I_D \times R_C \approx 0$, and the mobility enhancement factor $\gamma \approx 0$. Then $\sqrt{I_D} = \sqrt{w/(2L)\mu C_{OX}}(V_G - V_T)$, when $V_D > (V_G - V_T)$. Therefore, the data at highest V_D are selected, as shown in the left-hand graph in figure 2-15, and arrange the selected data as a transfer characteristic, as shown in the right-hand graph in the figure. From this transfer characteristic, the threshold voltage is the intercept with the x-axis and the transistor constant K can be obtained from the slope, as $K = 2 \times slope^2$. The threshold voltage V_T and transistor constant K extracted using this method are always used in the literature for comparison, and can be used as the initial values or limits for other extraction techniques. Note that the mobility enhancement and contact resistance are neglected, thus, the values for V_T and K are approximate.

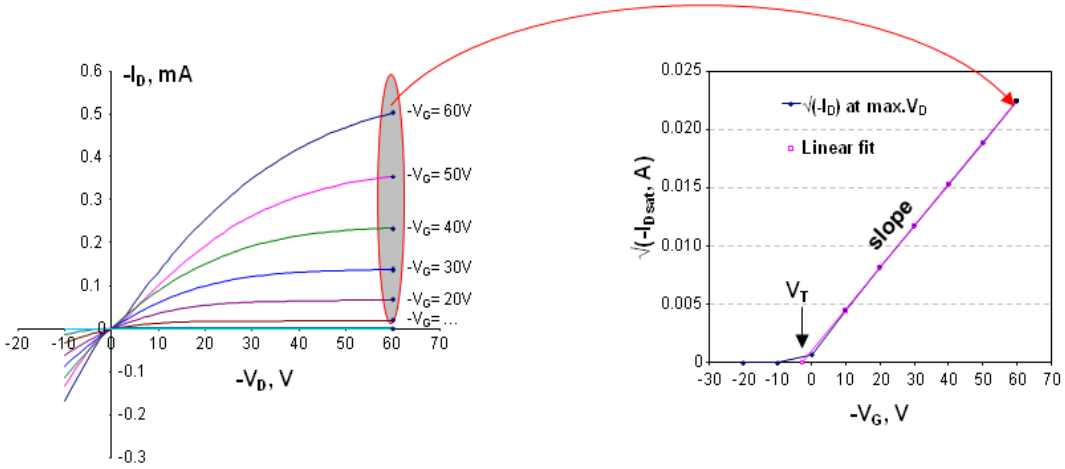

Figure 2-15 Saturation $\sqrt{I_D}$ vs. V_G extraction technique for output characteristic

2.2.3.2 Off-current (Leakage) at different V_D

The off-current for different drain bias voltages is extracted when the PTFT is well in the off state at very low gate bias voltage, for instance $-(V_G - V_T) \leq -10V$. For low $|V_D|$<5V and high $|V_D|$>55V, data selections are made at low V_G to make sure that the device is in the off state, assuming that the leakage current is not more than n × min I_D, e.g. n=3. For each of the selected ranges of V_D, calculate the average and the standard deviation of the leakage current. The off I_D is the average I_D +standard derivation/n in each set of selected data. Fig. 2-16 illustrates the procedure of the calculation, showing also that off I_D is different for different ranges of the drain bias voltages V_D.

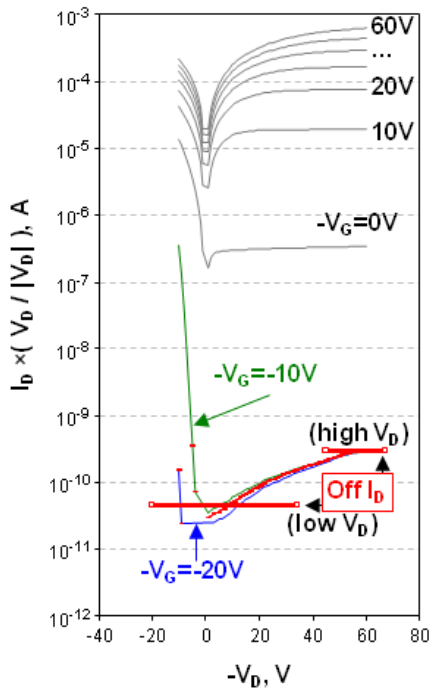

Figure 2-16 Leakage I_D from output characteristics of PTFT

The assumptions used here are reasonable for PTFTs, however, the measurement error may be large compared with the small leakage current, e.g. <1nA. Therefore, the off current can only be used to study the evolution by repeating the measurement under the same conditions, but should be carefully interpreted, when comparing off current evolutions under different conditions and between devices.

2.2.3.3 Transmission line model (TLM) method of PTFTs with changing length in the Linear Regime

This method is used to extract the contact resistance of PTFT with different lengths [45]. Comparing with the classic TLM method, the V_T, mobility enhancement factor γ and

transistor constant K should be known to make this method work for PTFT. The total resistance R_{DS} between the drain and source terminals of the PTFT operating in the linear regime is $R_{DS} = V_D / I_D$, when $|V_D| > 1V$, or $R_{DS} = \frac{\partial V_D}{\partial I_D}$, when $|V_D| \leq 1V$. Figure 2-17 shows variants of TLM, by including none or several parameters of the PTFT. The data are for PTFTs of channel lengths L=90, 190 and 370 micrometers, and at several gate bias voltages well above the threshold voltages of the PTFTs, thus, the PTFTs were operating well in the linear regime.

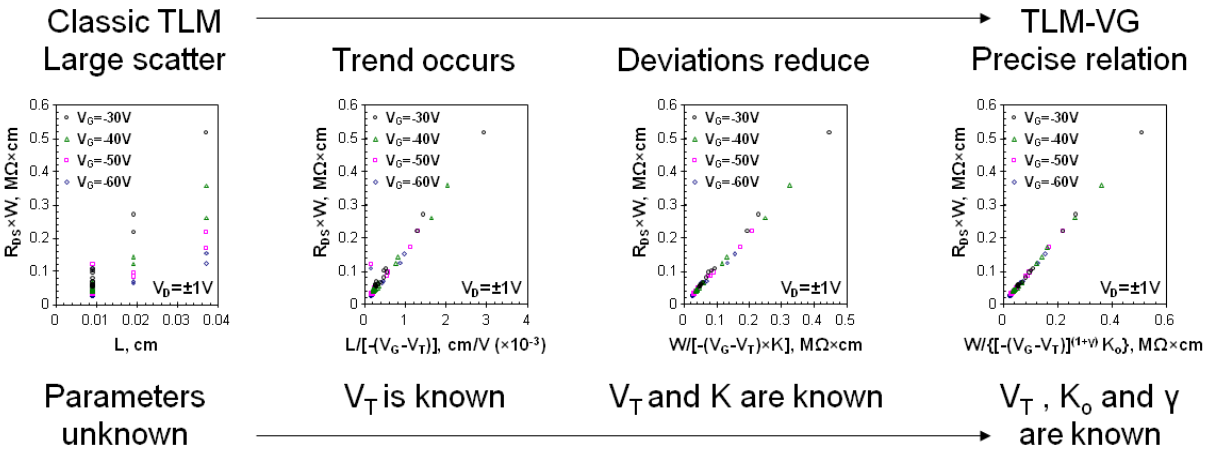

Figure 2-17 Improvement of TLM by including gradually the parameters of the PTFTs in the calculation of the intrinsic channel resistance, as reflected in the quantities at the x-axes of the TLM plots.

As shown in figure 2-17, from the left to the right, the classic TLM, $R_{DS}W$ vs. L results in big scatter which is because the threshold voltage V_T, mobility enhancement factor γ and transistor constant K are not the same in different devices, even if all the devices are fabricated simultaneously on the same substrate. However, when the threshold voltage V_T,

mobility enhancement factor γ and transistor constant K are all included in the calculations, then a precise linear relationship is formed.

2.3 Environmental and operational stability of PTFTs

The PTFTs always show some instability, when operating for prolonged time even in the inert environment or encapsulated. O_2 , H_2O, light, terminal bias voltage etc. may affect the device characteristic. The instabilities have been observed in virtually all organic materials, such as pentacene [25],[26],[46] ,P3HT [24], poly (thiophene) [47], P3OT [48] .There are a variety of mechanisms proposed to explain such instability, for instance, trap creation through all the volume of the polymer layer [26], defect generation, charge trapping, permanent/transient doping [24]. Several groups have reported that the reversibility of bias effects can take days, which indicates that such effect probably involves chemical mechanism [49],[50]. The P3HT PTFT exposed to O_2, H_2O, H_2O_2 and the white light exhibits increasing of both on and off currents. In addition, the nitrogen annealing at 160^oC can remove O_2, H_2O , and leads to decrease of the on and off currents [24]. The following sub-sections summarize the instability effects present in PTFTs by various operational and environmental conditions.

2.3.1 Threshold voltage

In consecutive measurements, the threshold voltage continuously shifts, which is probably due to the hole trapped at localized states. The thickness of the accumulated conduction channel is 3~5nm next to the insulator interface [25]. The traps might be

located in the entire volume of the thin film and created by the electrical field. Alternatively, thicker films can reduce the activation energy of interface traps and decrease the I_D [26].

The temporal varations of the threshold voltage can be described as a power-law function, $\Delta V_T \propto |V_G|^{\beta} t^{\gamma}$ [47],[49],[50], or an exponential function, $V_T(t)/V_T(t=0) \approx 1 - \exp[-(t/t_o)^{\beta}]$ of the time t [40]. The recovery of V_T can take days and can be accelerated by exposing the PTFT to light. In addition, PECVD silicon nitride and the thermal SiO_2 show similar threshold voltage shifts, while the defect density of silicon nitride is 5 orders higher than the thermal oxide, indicating that the organic semiconductor material, rather than the insulator material, dominates in the threshold voltage shifts. Possible origin for the V_T shift is a change in the structure of the organic material during the operation of the PTFT [51]. The temperature measurements show that below 220K, the threshold voltage depends only on temperature, while above 220K the threshold voltage varies also with the time. Furthermore, above 300K the drain current varies between devices, indicating impacts from the device fabrication [40].

Oxygen O_2 and water H_2O molecules diffuse into the P3HT thin film and create permanent and/or transient doping. The permanent doping can increase the hole concentration, consequently increasing the on and off currents and shifting the threshold voltage permanently. The transient doping induces temporal polarization effects, decreasing the hole concentration and causing the hysteresis in measurements with cyclic sweeps of the bias voltages The exposure to light probably affects the permanent doping,

the later converted from the transient doping previously created by the application of bias on the PTFT [24].

2.3.2 Mobility

PTFTs with different polymer thicknesses show different mobility. The thicker film has higher mobility, but $I_D$degraded more quickly with the time [26]. Encapsulated PTFTs maintain higher mobility, whereas the mobility in un-encapsulated pentacene TFT decreases by 30% after it has been stored at room environment for 500 hours, probably due to the H_2O absorption in the thin film [46] .

2.3.3 Subthreshold slope

The subthreshold slope is defined as $S = \frac{\partial V_G}{\partial(\log I_D)}$ in the unit of V/decade when $V_G < V_T$. The subthreshold slope is influenced by the organic material, because PTFTs with PECVD silicon nitride and thermal SiO_2 gate insulator layer have similar subthreshold slopes while the defect density of silicon nitride is 5 orders of magnitude higher than of the thermal oxide [51].

2.3.4 Contact resistance

A high contact resistance of PTFT results in poor performance of the PTFT. The contact resistance of PTFTs originates from the mismatch between the metal work function of the contact pads and the energy level of the highest occupied molecular orbital (HOMO) of the polymeric semiconductor. Another reason for high contact resistance is the disorder of

the organic film at the insulator and metal interfaces. Several groups have studied the contact effects in the PTFTs. The four probe conducting measurement has been used to study the contact resistance of PTFTs. The contact resistance and the channel resistance are decreased as the increasing gate bias, which agrees with the device with different length measurement [50]. However, proper pairing of metal and organic semiconductor, including monolayers at the contact, results in lower and virtually constant contact resistances in the PTFT, as desired.

2.4 Integration of PTFT with microfluidics

The influence of water and other chemical solutions on PTFTs has been studied by several groups [46],[52], either by coating the source and drain electrodes and dropping water on the device, or exposing the device to water. Both of these methods require removing the PTFT from the wet environment when measuring the electrical characteristics, because, the water solutions are conductive. Bao et al. have fabricated a microfluidic channel on the top of PTFTs [53]. However, the microfluidic channel was not across the entire channel of the PTFT. Therefore, the microfluidics parallel to the conduction channel of PTFT is necessary to study the sensitivity of the PTFT to water or other solutions.

Chapter 3 Fabrication of DKPP- βT PTFTs

The possibility of low-cost and large-volume mass production by printing of organic electronics, which can replace the expensive high-temperature vacuum technologies for crystalline semiconductors, is the driving force for the organic semiconductor research. Diketopyrrolopyrrole β-unsubstituted Quaterthiophene (DKPP-βT) is a novel high-mobility organic material, which is also suitable for solution-based processing by the fabrication of PTFTs. Therefore, PTFT based on polymeric semiconductor DKPP-βT are used in this study. The fabrication of the test devices is presented in the following sub-sections.

3.1 Materials

All the devices in this study are using bottom gated top contacted structures, as shown in figure 2-4(b). The contact resistance is small and the film is uniform. The substrates are 200nm SiO_2 coated heavily doped Si wafers, and are used as purchased.

3.1.1 Self assembly monolayer-OTS

A self assembled monolayer (SAM) has been demonstrated to improve the mobility of the OTFT [49, 54], [55]. Sirringhaus et al. [54] used methyl group ($C_6H_{19}NSi_2$, hexamethyldisilazane) which replaced the R_3Si-OH on SiO_2 surface, and improves the mobility of poly(3-hexylthiophene) (P3HT). Salleo et al. [49] has fabricated the organic thin film transistor (OTFT) on the same substrate using different SAM, including

octyltrichlorosilane (CH_3-$(CH_2)_{17}$-$SiCl_3$, OTS), which has the long alkane chain, and BTS (C_6H_5-CH_2-$SiCl_3$), which has the aromatic rings. OTS has proven to result in the highest mobility [49]. The molecules of both SAMs are perpendicular to SiO_2 and form a monolayer with the spacing between molecules bigger compared to SiO_2, as shown in figure 3-1. With the help of the suitable SAM, the polymer can form a well ordered lamellar structure which improves the $\pi - \pi$ stacking ordering in the charge transport direction, therefore, increases the mobility. For instance, regioregular polythiophenes, PQT, form lamellar stacking structure with the long side chain R regularly positioned on the backbone with the spacing approximately 1.2nm, as shown in figure 3-2 [55].

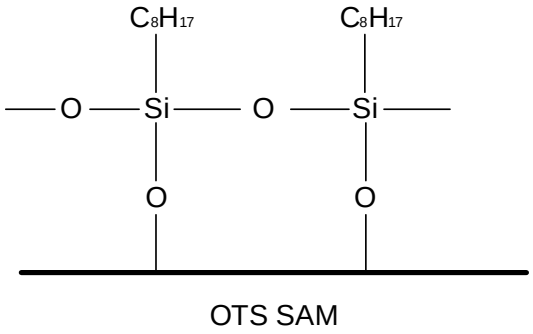

Figure 3-1 Schematic of OTS SAM on the surface of SiO_2

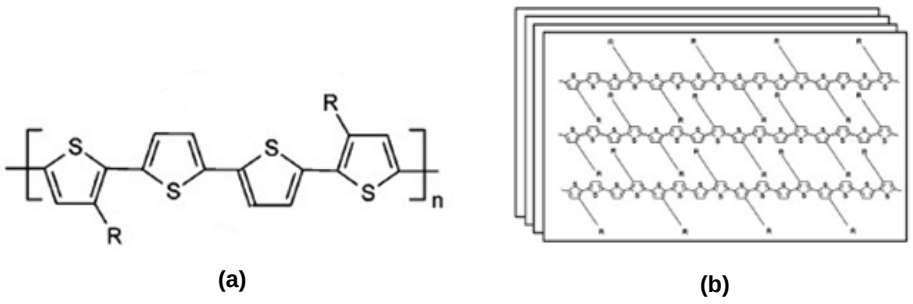

Figure 3-2 (a) Chemical structure of PQT (b) Lamellar stacking structure of PQT [55]

3.1.2 Semiconductor DKPP-βT

A full structure of semiconductor Diketopyrrolopyrrole β-unsubstituted Quaterthiophene (DKPP-βT) is shown in figure 3-3. It was reported high mobility 0.97cm^2/(Vs) with 100^{o}C post annealing and high molecular weight. However, the mobility was only ~0.35cm^2/(Vs) for the low molecule weight DKPP-βT even using the same fabrication process procedure as the high molecule weight one [56]. The bottom gate top contacted PTFT shows threshold voltage 6.5V, on/off ratio in the order of 10^6 [57]. Therefore, the high mobility, high on/off ratio, reasonable low threshold voltage, as well as the great printability for roll-to-roll, large volume, low cost manufacturing electronics make DKPP-βT promising.

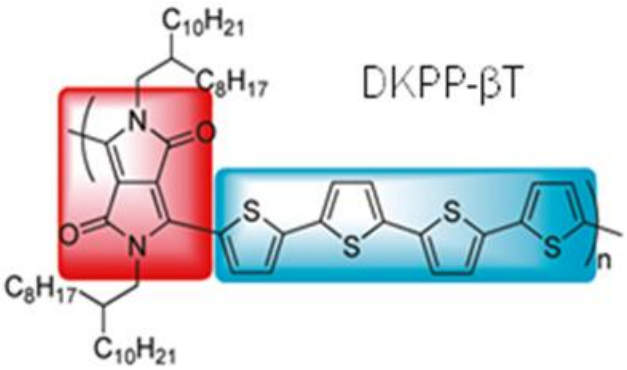

Figure 3-3 Structure of DKPP-βT[58]

3.1.3 Gold electrode

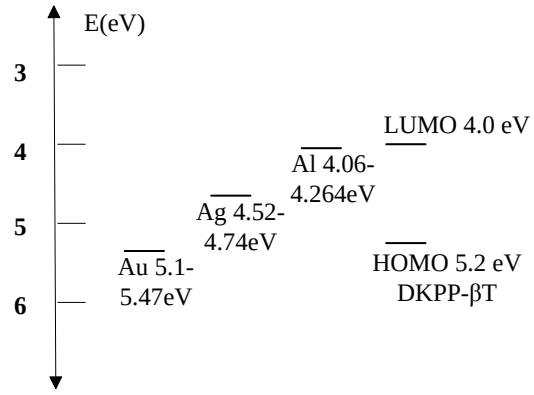

Figure 3-4 Comparison between the work functions of metals and HOMO/LUMO energy levels of DKPP-βT [58]

Because the DKPP-βT is a p-type semiconductor, holes serve as charge carriers. The hole injection barrier equals to the difference between metal work function and the highest occupied molecular orbital level of DKPP-βT. The work functions for Al, Ag, Au are 4.06-4.26 eV, 4.52-4.74 eV, 5.1-5.47 eV, respectively. The energy level of the lowest unoccupied molecular orbital and the highest occupied molecular orbital for DKPP-βT are 4.0eV and 5.2eV [58], as shown in figure 3-4. Hence, among the commonly used metals for contact to organic semiconductors, the work function of gold gives the smallest injection barrier and the most of the PTFTs use gold as the source and drain electrodes.

3.1.4 PDMS

Polydimethylsiloxane (PDMS) has been used in microfluidics fabrication for decades, because of its transparency, ease of fabrication and environmental stability. Also, PDMS has good leak-proofness that guides the liquid within the channel, which is proper for the

fabrication of the microchannel on PTFTs. The base and curing agent of PDMS were purchased from Dow Corning Inc. by the distributor in Canada (5109 Harvester Road, Unit B3, Burlington, ON L7L5Y9). The PDMS base will polymerize and cross link after mixing with the curing agent and the heating accelerates the polymerization. The cross linked PDMS is a hydrophobic solid elastomer [59]. The hydrophobic surface makes the polar molecule (such as water) difficult to absorb in the PDMS, consequently proper for the microfluidics. The ratio of base and curing agent is 10:1, as the supplier suggested, for the microchannel as well as the binding agent used in micro-contact printing. More curing agent and higher spinning speed gives thinner layer of binding agent, since the width of the microfluidic channel is 200μm which is large, and the ratio of 10:1 of the base and curing agent gives good result.

3.2 Fabrication methods

3.2.1 PTFTs fabrication

The fabrication process flow of top-contacted bottom-gated DKPP-βT PTFT is going to be described in the following sub-sections. The substrates are 200nm SiO_2 coated heavily doped Si wafers.

3.2.1.1Aluminum gate electrode

The SiO_2 side of the SiO_2 coated heavily doped Si wafer (n+ Si) was protected with 0.8μm positive photoresist IS1808, spinning 4000rpm for 30seconds and baking at 130^{o}C for 2 minutes. Then immerse the wafer in hydrofluoric acid (HF) buffer solution for 2.5

minutes to remove the silicon oxide. After that, 200nm aluminum was sputtered onto the n+ Si side of the wafer, to guarantee a good electrical contact with the chuck of the probe station during the measurements. Then, the photoresist was removed using acetone and methanol.

3.2.1.2 Substrate preparation

The wafer was cut into pieces and immersed in isopropanol (IPA) for 5 minutes and washed using IPA followed by the air blow dry. After that the wafer was cleaned using air plasma for 2 minutes and immersed in IPA for another 5 minutes again. Then it was rinsed using IPA and followed by dry air blow again.

3.2.1.3 Substrate surface modification

1ml OTS was dissolved in 40ml toluene and the prepared wafer pieces were immersed in the solution heated at 60^{o}C for 20 minutes in the covered petridish. Then the wafer was rinsed with toluene twice followed by IPA wetted cotton tip wiping, finally dry air blew the wafer.

3.2.1.4 Solution preparation and film deposition

0.5% wt semiconductor material DKPP- βT (Xerox Research Centre of Canada, XRCC) was dissolved in 1,1,2,2, Tetrachlorethane and heated to 60^{o}C for 1 hour to make it fully dissolved. During the heating, the solution was covered using aluminum foil, because DKPP- βT is light sensitive. Finally, the semiconductor solution should be the mazarine

blue and filtered through a 1 micron syringe filter quickly to remove the undissolved polymer.

The mazarine blue solution was dropped onto the modified substrate and spun immediately at 2000rpm for 1 minute. After that, the film deposited substrate was left in the vacuum oven (in the order of several mbar) at 70^{o}C for an hour to evaporate the remained 1,1,2,2, Tetrachlorethane within the film, followed by post annealing to 140^{o}C. Then the substrate was left in the vacuum oven overnight to cool down to room temperature. Post annealing can improve mobility, subthreshold swing, on/off ratio, which probably result from the better crystallization of the polymer [24]. The thickness of flat thin film is about 30 nm.

3.2.1.5 Electrode deposition

The source and drain gold electrodes were deposited onto the top of the semiconductor film using vacuum evaporator Edward E306A Coating System through a metal shadow mask. The substrate was held at room temperature during the evaporation. The thickness of gold is 120nm. The dimensions of the PTFTs are 40μm×1000μm, 90μm×1000μm, 190μm×1000μm, 370μm×1000μm, 40μm×5000μm, 90μm×5000μm, 190μm × 5000μm, and 370μm × 5000μm, respectively.

The size of the microfluidics PTFT is larger, as shown in figure 3-6, allowing for manual alignment of the microfluidic channel. The shadow mask, as shown in figure 3-6 was

designed using Adobe Illustrator and cut into transparency by Craft Pobo Pro from Graphtec.

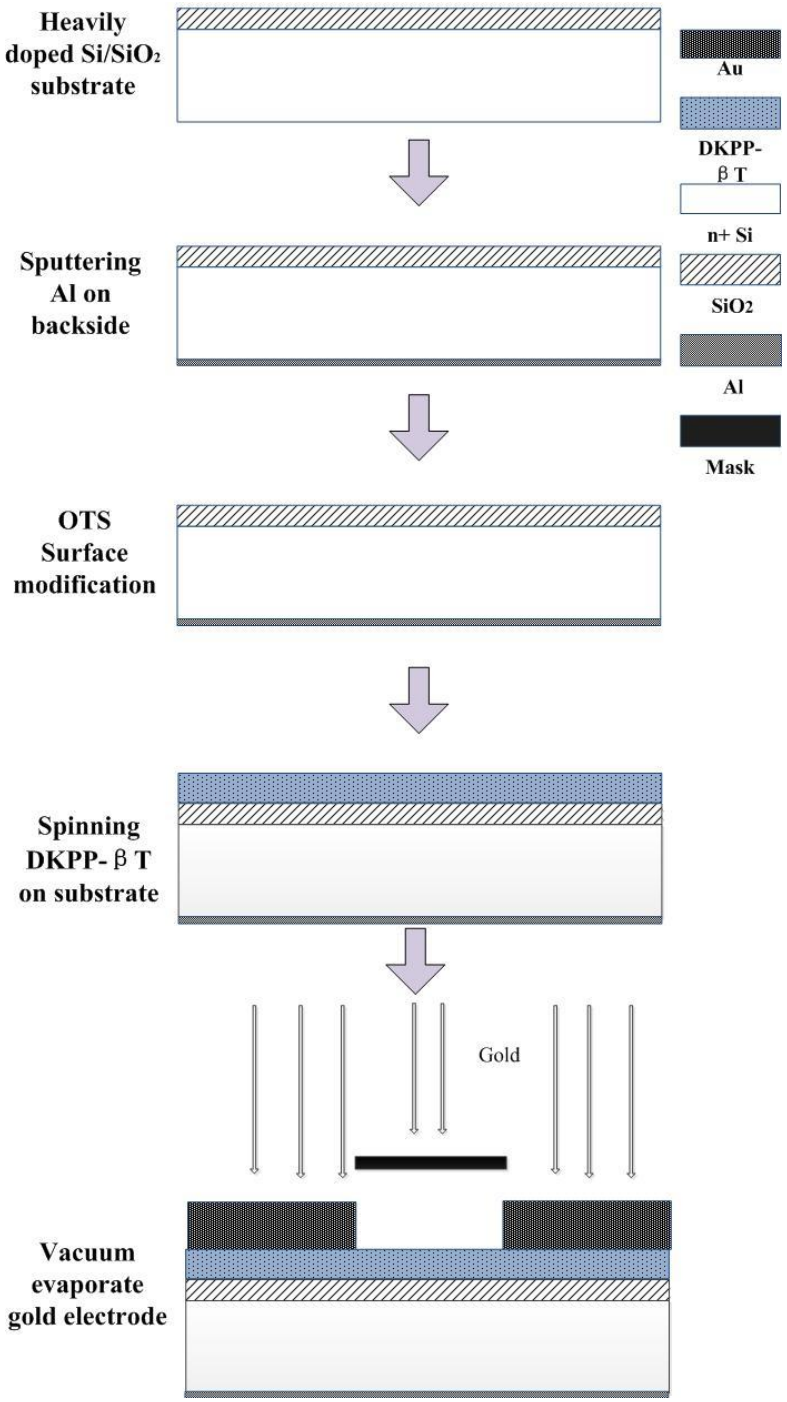

Figure 3-5 Fabrication process flow of DKPP-βT PTFT

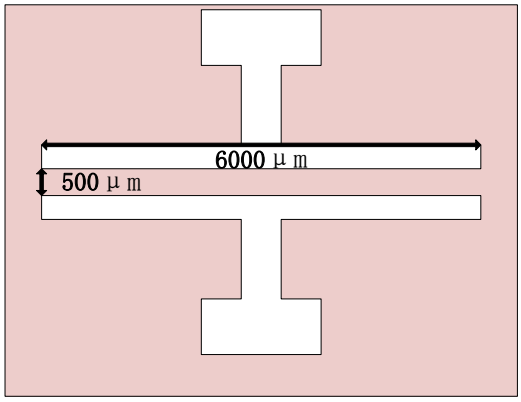

Figure 3-6 shadow mask design for gold electrodes (not to scale), W/L=6000 μm /500 μm

3.2.2 Integration of PTFT with microfluidic channel

To study the stability of DKPP-βT PTFT under liquid environment, microfluidic channel was integrated on the top of the PTFT. The mask for the microfluidic channel is shown in figure 3-7.The fabrication process of integration of the microfluidic channel on the top of the DKPP-βT PTFT is shown in figure 3-8.

3.2.2.1 PDMS master mold fabrication

The mask for photolithography of PDMS master mold was designed by using L-edit and printed on transparency using Fineline Imaging, as shown in figure 3-7. The dimensions of the channel are 200μm×10mm. The mold for the microfluidics channel was prepared using Si wafer.

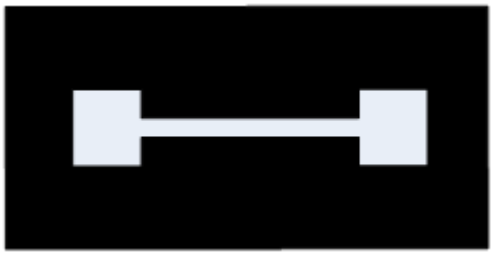

Figure 3-7 Schematic of mask design for PDMS mold (not to scale)

The Si wafer was cleaned by immersing in acetone and methanol for 1 minute respectively and rinsed in DI water for 5 minutes, followed by dry air blow and heated at 110^{o}C for 2 minutes. After that, 50 Watt/ 1minute oxygen plasma was used to remove the remaining inorganic particles from the surface of the wafer. Negative photoresist (SU-8) was dropped on the surface of the wafer uniformly and spun at 500rpm for 20 seconds, followed by 2750 rpm for 40 seconds. Prebake the wafer at 65^{o}C for 15 minutes and at 95^{o}C for 30 minutes. Expose the wafer to UV light at total exposure energy of 600 mJ/ cm^{2}. Post-bake the wafer at 65^{o}C for 1 minute and increase to 95^{o}C for 10 minutes. Immerse the wafer in the developer and wait for the features became clear and all the other photoresist washed away. Finally, wash the wafer using DI water and dry it with nitrogen blow. The thickness of the channel is ~100μm.

3.2.2.2 PDMS microchannel fabrication

The PDMS base and curing agent was mixed as 10:1 dropped onto the master mold and heated at 80^{o}C for 2 hours. After the PDMS well cross linked, it was peeled off from the mold and 2 holes were punched on the 2 squares of PDMS in figure 3-7 using 1.5μm

diameter hole puncher. The holes were used to connect with tubes. Then the PDMS base and curing agent mixture was cast onto the clean wafer and spun at 6000rpm for 2 minutes. The top of cured PDMS channel was put on the thin film of liquid PDMS and lifted off, allowing the microchannel bond to the PTFT and covering source and drain electrodes simultaneously.

3.2.2.3 Microchannel integrated with PTFT

The PDMS microchannel with binding agent was aligned and attached to the PTFT under microscope and the binding agent covered the source and drain electrodes. The integrated device was covered with aluminum foil and left at room temperature overnight for the curing of the PDMS adhesive.

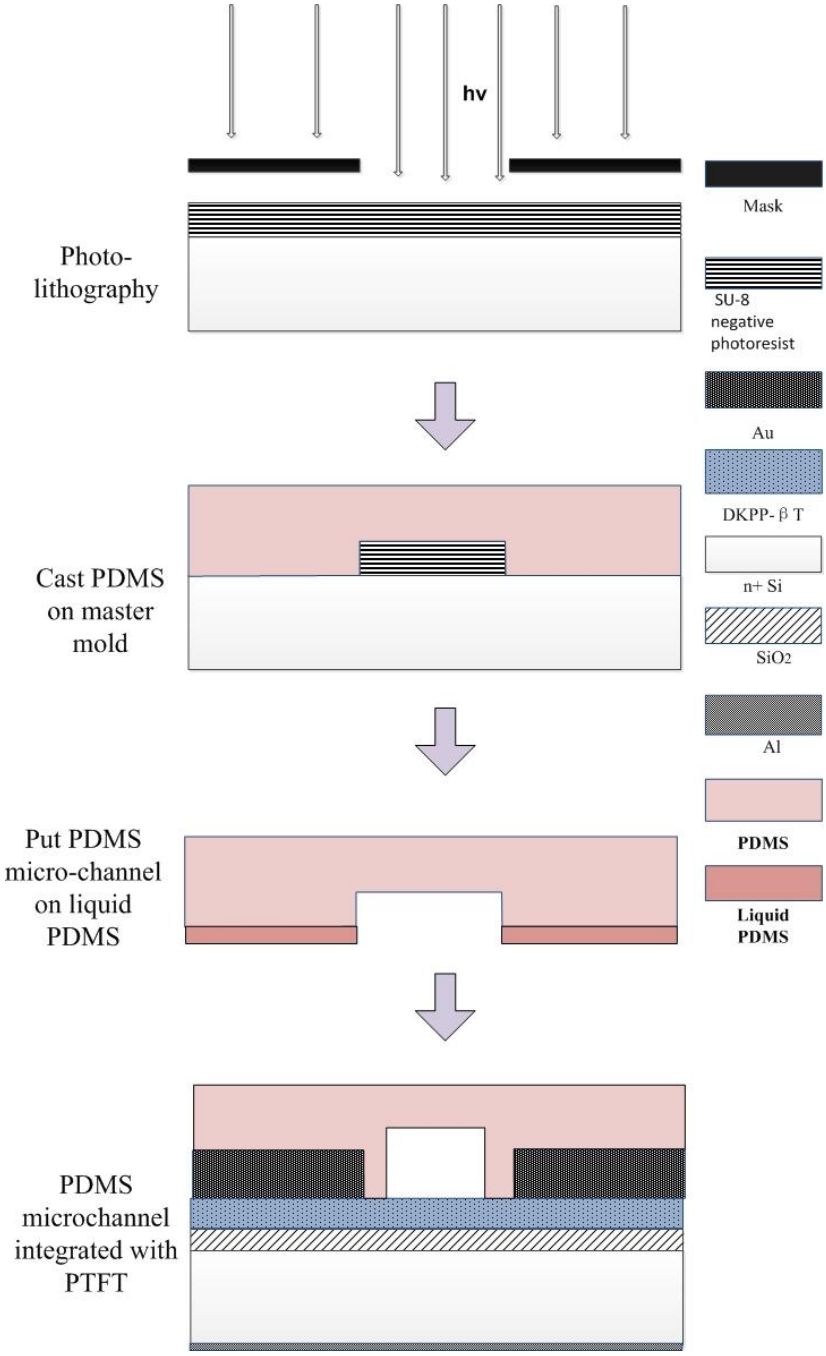

Figure 3-8 Fabrication process flow of PDMS micro-channel and integration with DKPP-βT PTFT

Chapter 4 Experimental Studies

4.1 Methods for study

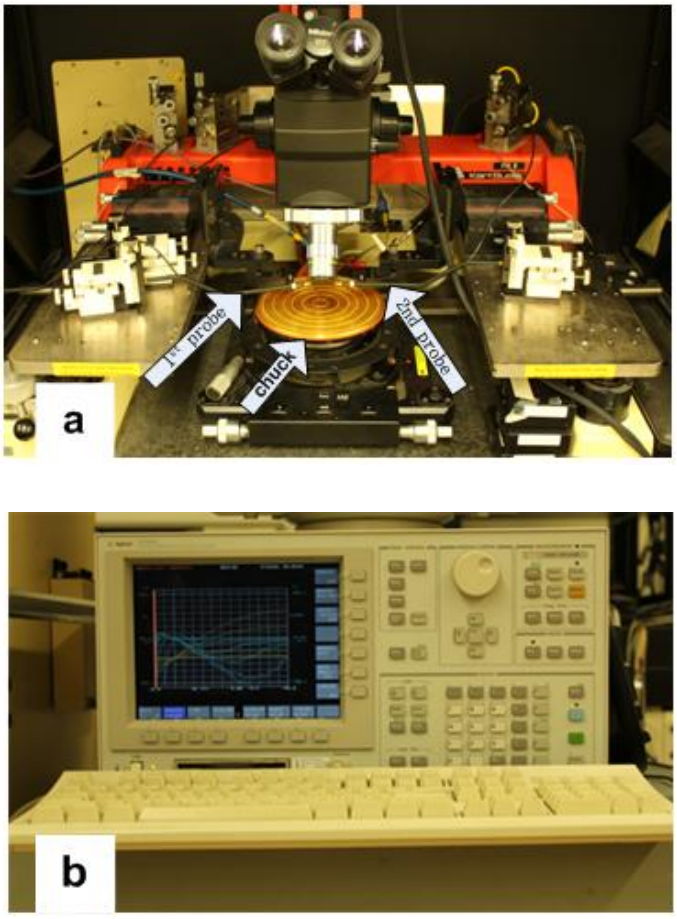

Figure 4-1 Measurement setup a) Probe station from Karl Suss b) Agilent 4156C precision semiconductor parameter analyzer

The PTFTs were measured in air without any encapsulation. The chuck held the PTFT providing the gate bias and the two probes placed on the source and drain electrodes providing source and drain bias voltage respectively. The chuck and probes connected

with semiconductor parameter analyzer which generated the bias voltage and measured the device currents. In the output characteristic measurements, the drain bias voltage V_D was swept from 20V to -60V with -1V step at gate bias voltages V_G from 20V to -60V with -10V step and source bias voltage $V_S = 0V$. In the transfer characteristic measurements, gate bias voltages V_G was swept from 20V to -60V with -1V step at drain bias voltage V_D = -1V and -60V and again source bias voltage $V_S = 0V$. The measured data have been stored and analyzed using the extraction techniques described in section 2.2.

4.2 PTFTs under illumination

Figure 4-2 illustrates the result from consecutive measurements of the transfer characteristics of the PTFT in dark and under illumination. The PTFTs were measured in dark from measurement No. 1 to No.16, collecting the evolution with time, in which the threshold voltage ($-V_T$) increased. Following the measurements from No.17 to No. 26 have gathered the impact of illumination. The illumination ($0.18mW/cm^2$) reduces the threshold voltage ($-V_T$) in measurement No.21 and the higher light intensity ($0.47mW/cm^2$) reduces the threshold voltage ($-V_T$) more in measurement No. 25, simultaneously reducing the slope of the curve. Finally the PTFT was measured again in dark collecting the recovery behavior after illumination. In measurement No.26, the threshold voltage ($-V_T$) recovers towards the initial value before the illumination, but the slope remains low.

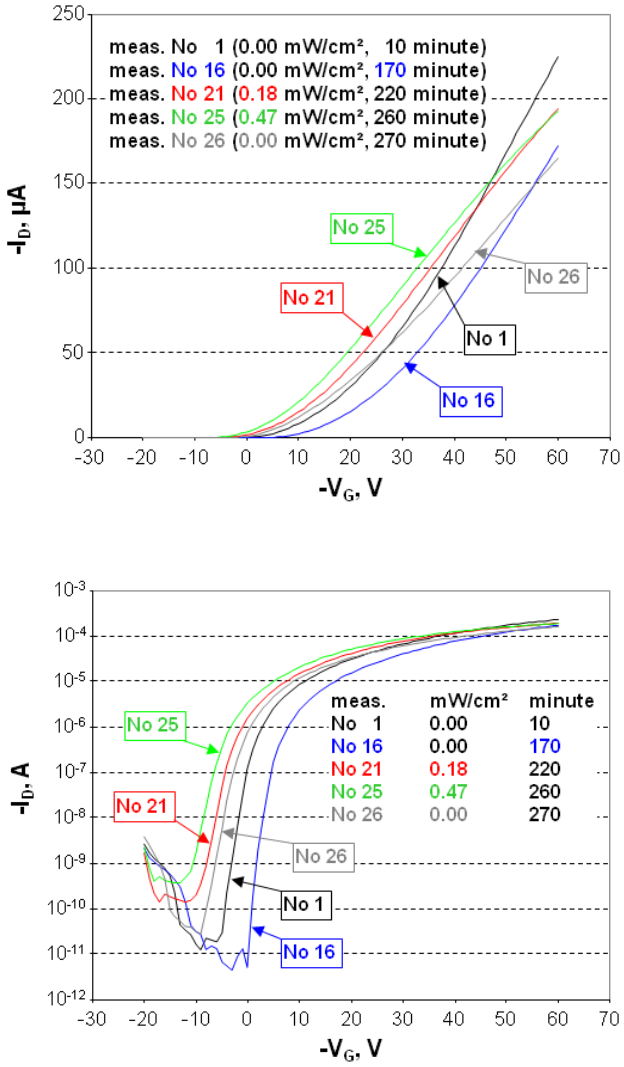

Figure 4-2 Transfer characteristics of PTFT (W/L=3500μm/ 90μm) in the saturation regime ($-V_D$=60V) measured in dark and under illumination with white light

The overall evolution with time is: (1) the threshold voltage $-V_T$ increases; (2) the drain current $-I_D$ decreases; while (3) the light decreases the threshold voltage $-V_T$ and increases the off current, but it does not increase $-I_D$ at high V_G.

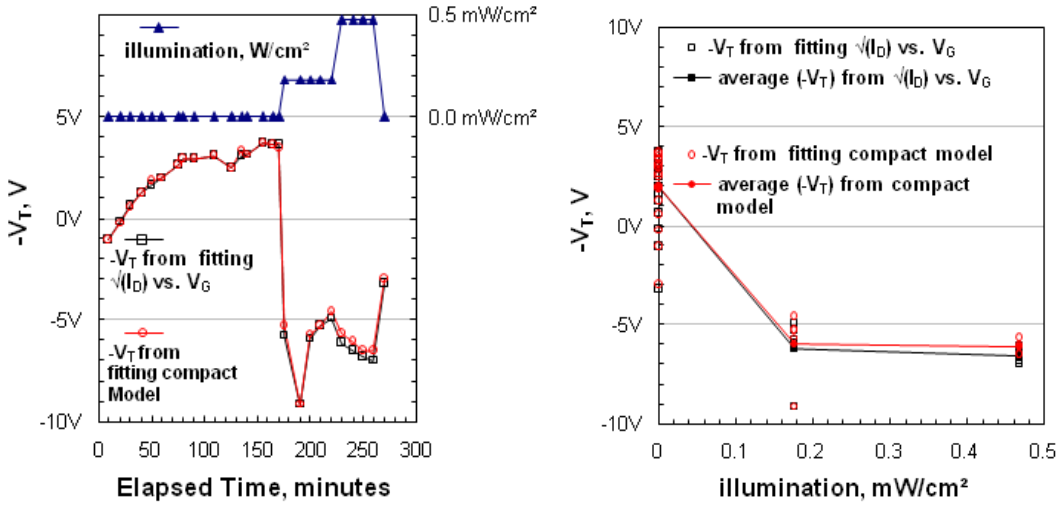

Figure 4-3 The threshold voltage $-V_T$ variation with the time under dark and illumination

The threshold voltage $-V_T$ variation is the main effect in this measurement. Firstly, $-V_T$ increases nonlinearly with time during the measurement, which due to the charge build-up within the semiconductor material [51]. Secondly, $-V_T$ decreases under illumination, where the light acts as an "additional gate bias".

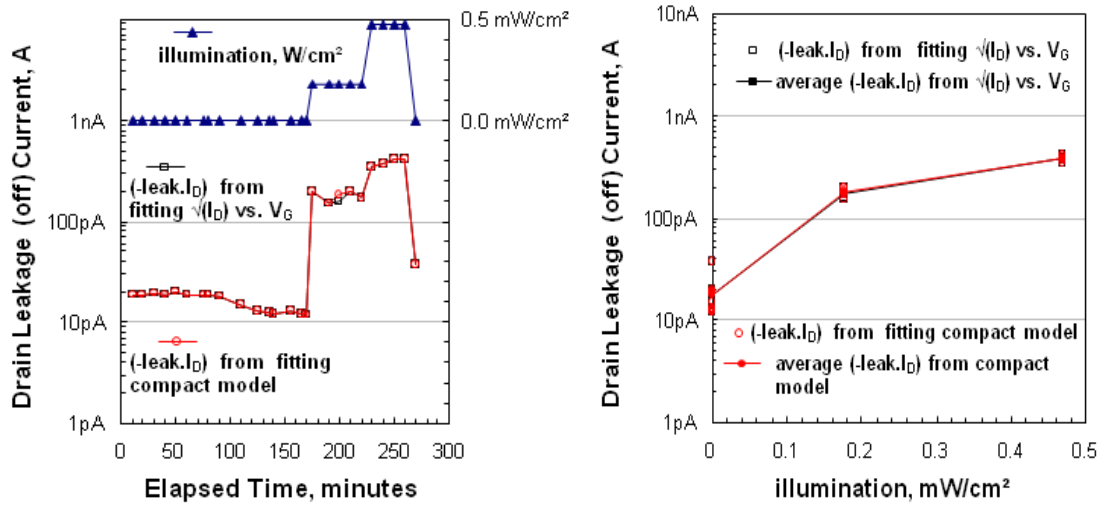

Figure 4-4 The off drain current evolution with the time under dark and illumination

The drain leakage current is calculated as described in section 2.2. As shown in figure 4-4, the off current is sensitive to the light and the off $-I_D$ changes proportionally with the light intensity. The off current also seems weakly dependent on time.

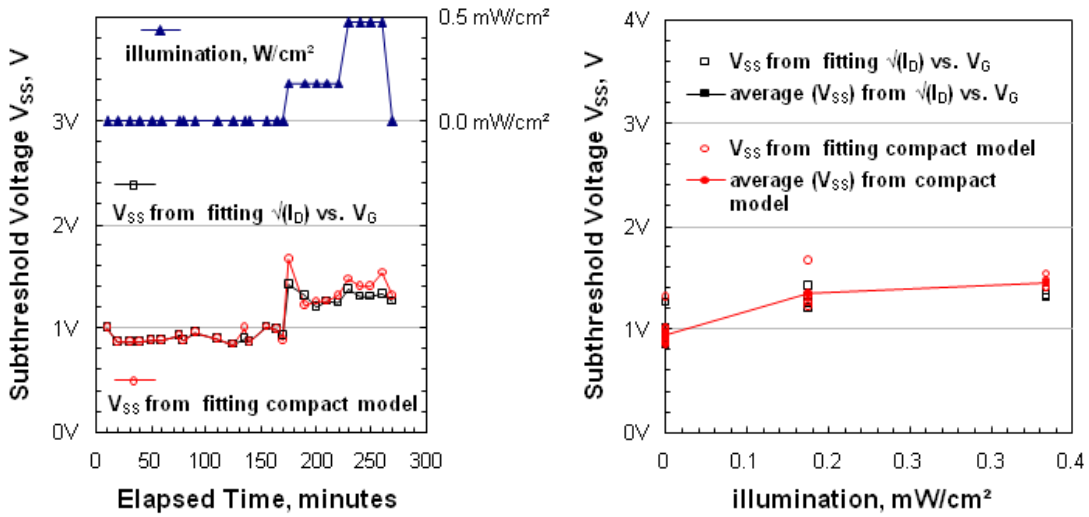

Figure 4-5 The subthreshold voltage evolution with time under dark and illumination

The subthreshold voltage is also sensitive to light; however, the dependence is weak and not proportional to the light intensity. The subthreshold voltage is not dependent on the measurement time.

To prove the light effect on the PTFTs, more measurements were performed with variant intensity of illumination, which were dark, 0.111mW/cm^2, 0.138mW/cm^2,0.176mW/cm^2, 0.225mW/cm^2, 0.281mW/cm^2, 0.382mW/cm^2, $0.469\ \text{mW/cm}^2$ respectively. The width and the length of the device were 5000μm and 90μm, respectively. The consecutive measurements were 17 measurements in dark, 6 measurements under the lowest intensity of illumination, 5 measurements in the dark, illumination applied starting from the lowest

to the highest with 4 measurements for each illumination condition, and 9 measurements in dark finally, as shown in figure 4-6.

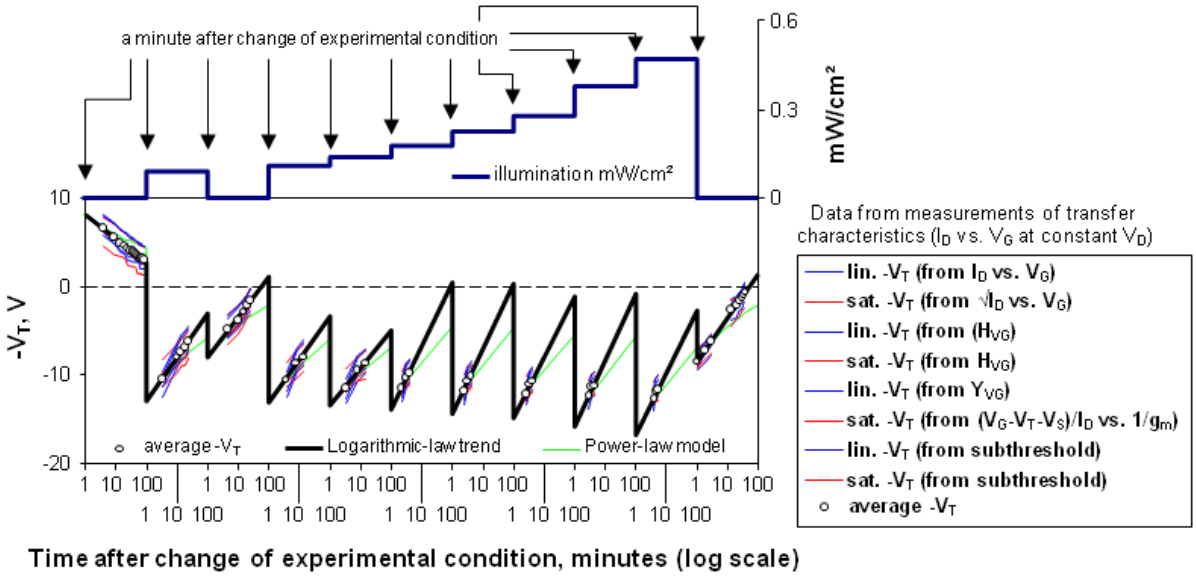

Figure 4-6 Threshold voltage evolution under different intensity of illumination

The evolution of the threshold voltage is drawn against the logarithm of time after changing of experimental condition in minutes. The threshold voltage is not linearly changing with the time; therefore, we propose different trend models to fit the changes.

First, the logarithmic trend is proposed, as

$$V[\log(t)] = V_o + S_{10} \lg\left(\frac{t}{t_o}\right)$$

where $V_o = V_T(t_o)$ at $t_o = 1$ minute , $V_\infty = V_T(t_\infty)$ at $t_\infty = 100$ minutes $\gg t_o$, $S_{10} = \text{Slope}_{10} = \partial V_T / \partial \log_{10}(\frac{t}{t_o})$ in the unit of [V/dec] . The logarithmic trends seems to be applicable to the measurement data, however, V_∞ varies.

Power- law model is proposed as

$$\frac{V - V_\infty}{V_o - V_\infty} = (\frac{t}{t_o})^\alpha \Rightarrow \ln\left(\frac{V - V_o + V_o - V_\infty}{V_o - V_\infty}\right) = \ln\left(1 + \frac{V - V_o}{V_o - V_\infty}\right) \approx \frac{V - V_o}{V_o - V_\infty} \approx \alpha \ln\left(\frac{t}{t_o}\right)$$

$$\Rightarrow V \approx V_o + (V_o - V_\infty)\alpha \ln\left(\frac{t}{t_o}\right)$$

where $\ln(1+x) \approx x$ at $x \approx 0$ and α is constant (~-0.18). A power law model also fit the measurement data, but is too slow at t_∞.

Comparing the different models in figure 4-7, both of the two models can fit, but neither is perfect. The average of the threshold voltage shows stable trends, however, in each data set there is scattering. As shown in figure 4-8, the initial threshold voltage V_o at the first minute after a change of an experimental condition, follows a linear relationship with the illumination intensity, which is 10~12 V/ (mW/cm^2).

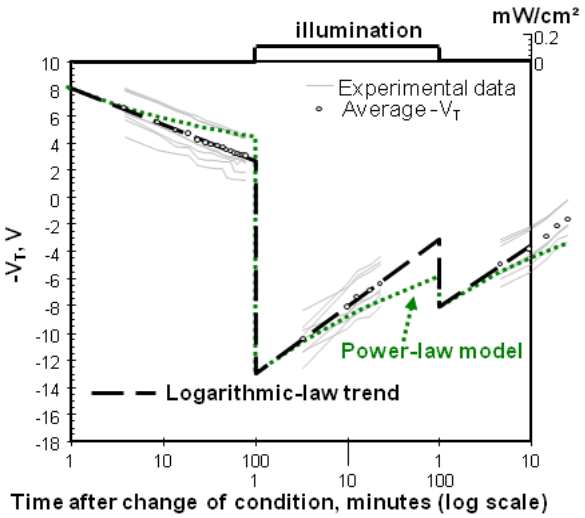

Figure 4-7 Different trends for the threshold evolution of time

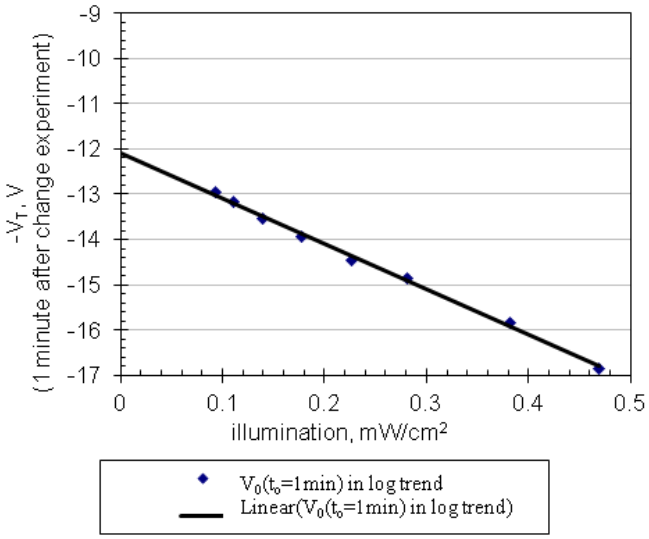

Figure 4-8 Initial - V_T after 1 minute of experimental condition change

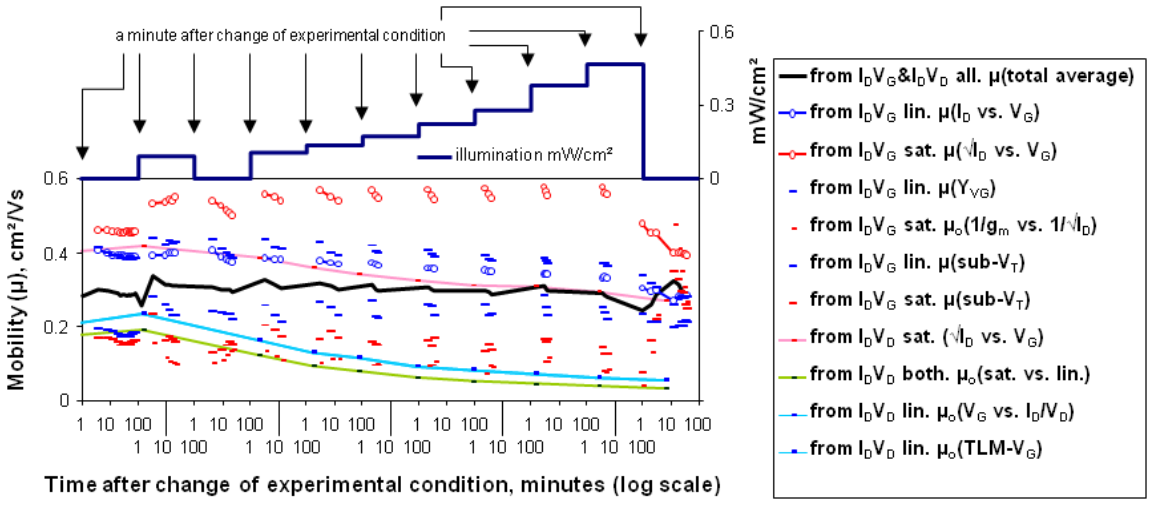

Figure 4-9 Evolution of the mobility under different intensity of illumination as obtained from several characterization techniques

The symbols in figure 4-9 depict the values for the carrier mobility and are obtained by several extraction methods. The illumination increases the spread between the values extracted by the different characterization techniques, while the time seems is reducing the spread. However, the average line (thick black line) in figure 4-9 shows that the average value of mobility is unchanged during the long time measurements, as well as under different illumination conditions, which is beneficial for the PTFT.

In illumination measurements, the threshold voltage reduction, off current and the subthreshold slope increase, unchanged mobility also have been observed at [60],[61]. The photons are absorbed in the polymer and the excitons are generated [62]. When the photon energy beyond the energy difference between trap state and transport band edge, the trapped charge carriers are released [36] and move under electrical field, reducing the threshold voltage. However, in the same condition consecutive measurements, the charge

carriers are trapped in the localized states and threshold voltage is increased. Also, the increase of carrier density raises the conductivity of polymer, and therefore increases the off current and subthreshold slope. However, the light effect is negligible at high gate bias when the PTFT in strong accumulated regime [63].

Figure 4-10 shows the TLM plot obtained after using the transmission line model to extract the contact resistance of PTFTs with different lengths measured both in dark and under illumination. The contact resistances are extracted at different gate bias when $(-V_G) > (-V_T)$. The y-intercept in the graph $R_{DS} \times W$ vs. $\frac{L}{\mu_o C_{OX}(V_G - V_T)^{1+\gamma}}$ gives $R_C \times W$. The lengths of the devices are 40μm, 90μm, 190μm, 370μm and the width is 5000μm. All the data points from different bias voltages, devices and illumination intensities align with single linear relationship, which is shown in figure 4-10. The single y-intercept implies that despite the variations in the threshold voltage, mobility, and mobility enhancement factor, the contact resistance is the same in PTFTs from one substrate and the illumination does not change the contact resistance. The contact resistance is inversely proportional to the width of the device, $R_C W$ equals to $5.4 \times 10^3 \Omega$cm (channel width 0.5cm). The unique intercept in figure 4-10 also implies that the contact resistance is Ohmic and bias independent, as desired, while very often in the literature undesirable gate bias-dependent non-linear contacts in OTFTs are reported [50],[64].

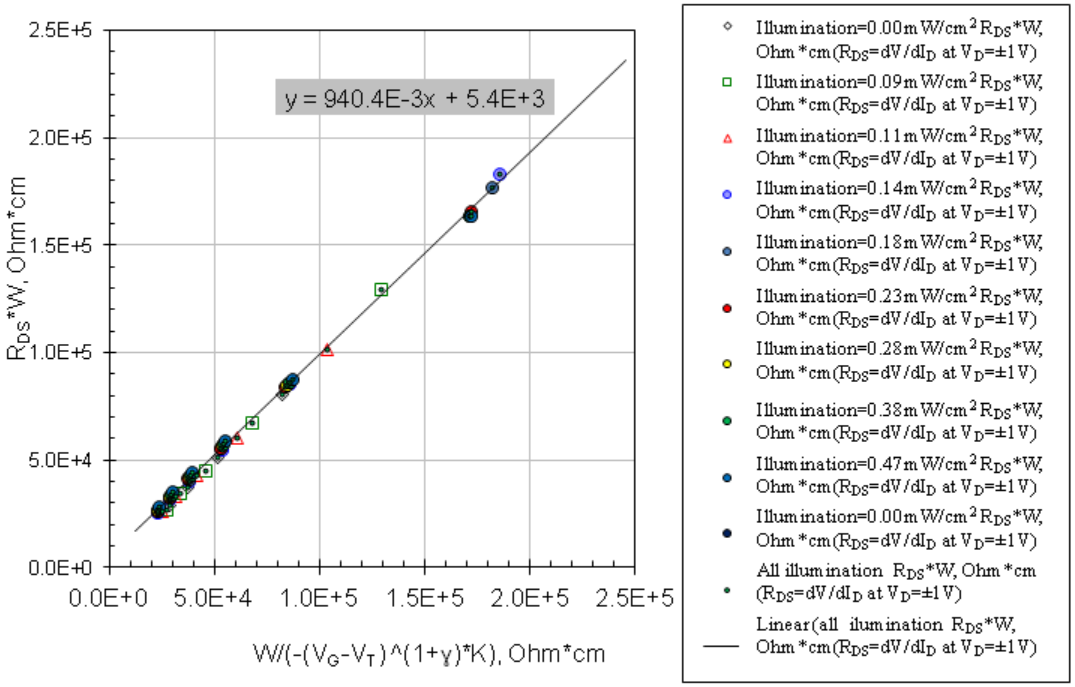

Figure 4-10 Transmission line model for the contact resistance extraction

4.3 Microfluidics PTFTs

4.3.1 Device with DI water in the microfluidics channel

The DKPP-βT polymeric thin film transistor shows high mobility (~0.3cm^2/Vs) and the repeatability of PTFT fabrication enable the integration of the PTFT with microfluidics channel. The width and length of the microfluidics PTFT are 6000μm and 500μm. The microchannel can guide the DI water or other solutions flow through the surface of the semiconductor DKPP-βT, the microphotograph is shown in figure 4-11. This integrated device allows only the semiconductor channel, rather than the drain and source electrodes,

exposed to liquid analytes during operation, and enables studying the sensing property of the DKPP-βT PTFT.

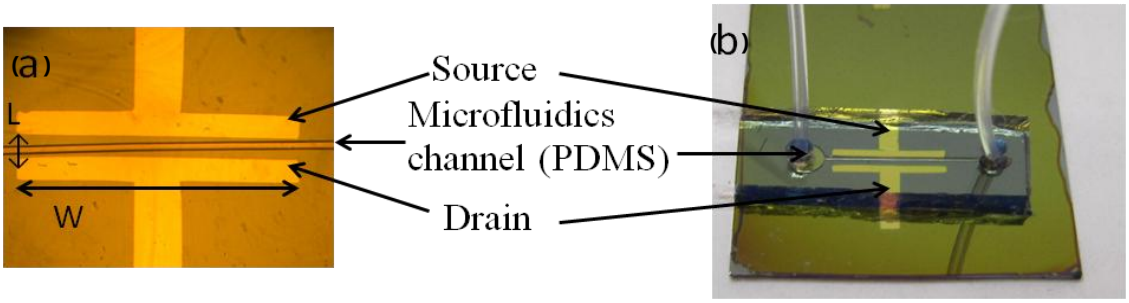

Figure 4-11 (a) Microphotograph of the PTFT with W/L=6000μm/500μm integrated with the microfluidics channel. (b) Picture of the microfluidics PTFT.

The deionized water (DI water) is from the clean room of the Centre for Emerging Device Technologies (CEDT), McMaster University. The electrical properties were measured using Agilent 4156C precision semiconductor parameter analyzer.

Firstly, 20 consecutive transfer characteristics (I_DV_G) measurements of the microfluidics PTFT were performed with air (without DI water) in the microfluidics channel. These 20 measurements are denoted as Air Trial 1. Then DI water was injected flowing through the microfluidics channel using syringe. Another 20 consecutive transfer characteristics (I_DV_G) were measured with DI water in the microfluidics channel, and denoted as Water trial 1. The above experiments are repeated several times, alternating injection of air and DI water in the microfluidics channel, and the sets of 20 measurements of transfer characteristics are denoted as Air/Water Trial 2, 3 and so on. In figure 4-12, the drain current of the second measurement in DI water from trial 1 slightly decreased at high gate

bias voltage comparing with the last measurement in Air trial 1.The detailed threshold voltage, mobility, subthreshold slope and off current evolutions are discussed on below.

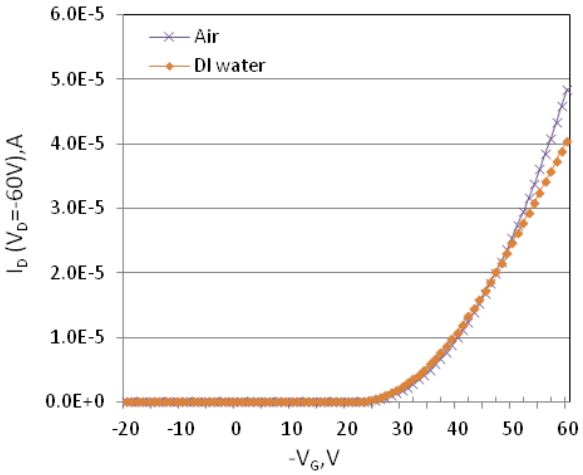

Figure 4-12 Transfer characteristics of PTFT in the saturation regime (V_D =-60V). Air indicates the last measurement in Air trial 1, DI water indicates the second measurement in Water trial 1.

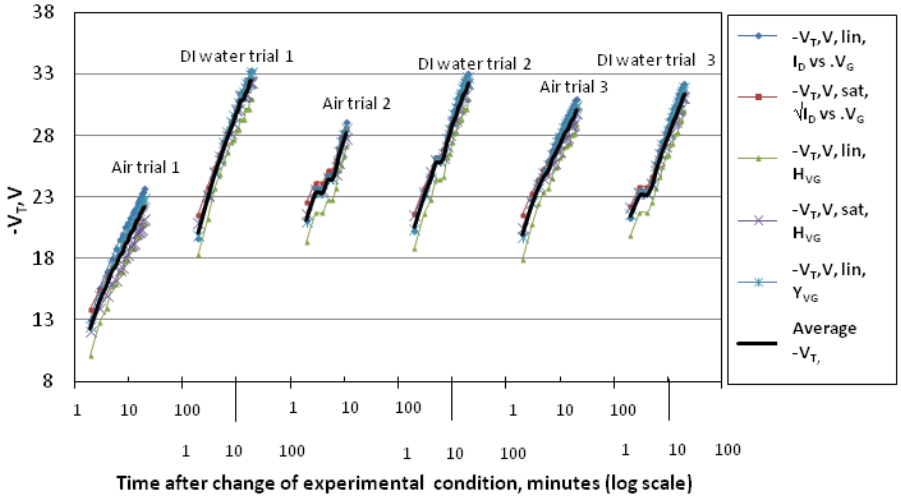

Figure 4-13 Threshold voltage evolution (V_D =-1/-60V, V_G =±20~-60V)

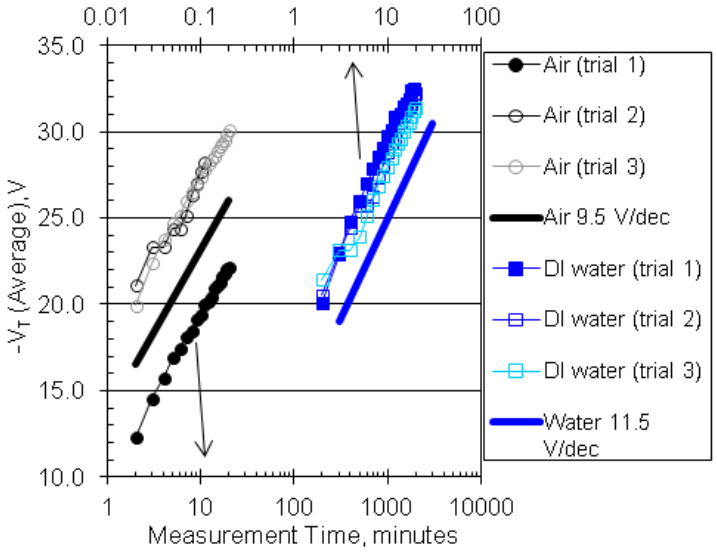

Figure 4-14 Evolution of the average threshold voltage from operation of the PTFT in the linear ($-V_D$ =1V) and saturation ($-V_D$ =60V) regimes

During the continuous operation, both with and without DI water in the channel, the threshold voltage increases to more negative value. The average threshold voltage V_T vs log (t) falls into a quasi linear relationship; hence, the logarithmic trend is defined as

$$V_T(\log(t)) = V_{T0} + S \times \log\left(\frac{t}{t_o}\right)$$

where t_o = 1minute corresponds to $V_{T0} = V_T(t_o)$, the slope $S=\partial V_T / \partial \log\left(\frac{t}{t_o}\right)$ is in unit V/decade (V/dec). The slope of the air trials is 9.5V/dec, while the slope of the DI water trials is 11.5V/dec, slightly steeper than for trials in air. The water molecules permeate the polymer and settle at the grain boundaries. Water at grain boundaries trap hole carriers [65],[66], therefore, slightly increases the slope of V_T vs log (t).

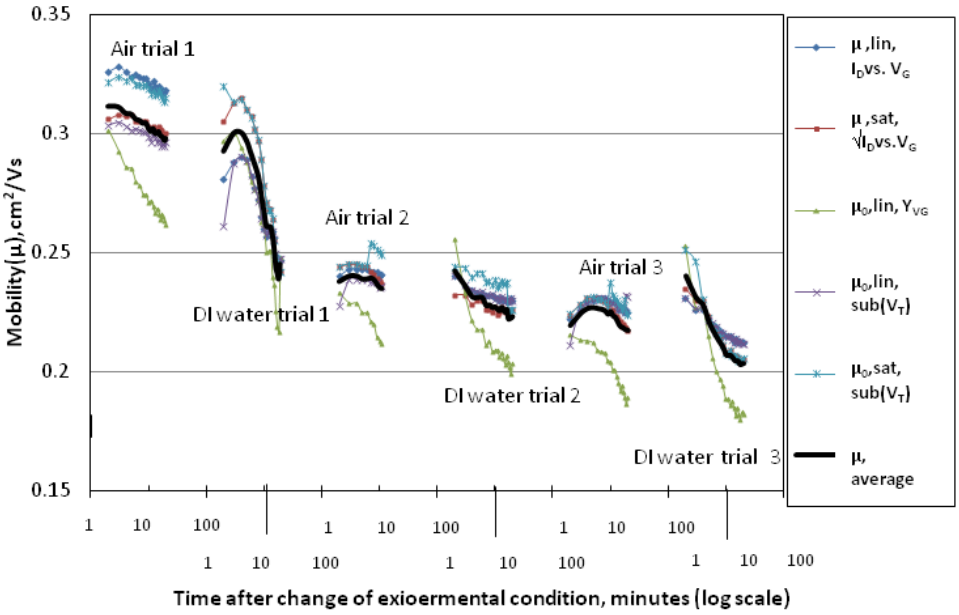

Figure 4-15 Mobility evolution in microfluidics PTFT (V_D =-1/-60V, V_G =±20~-60V)

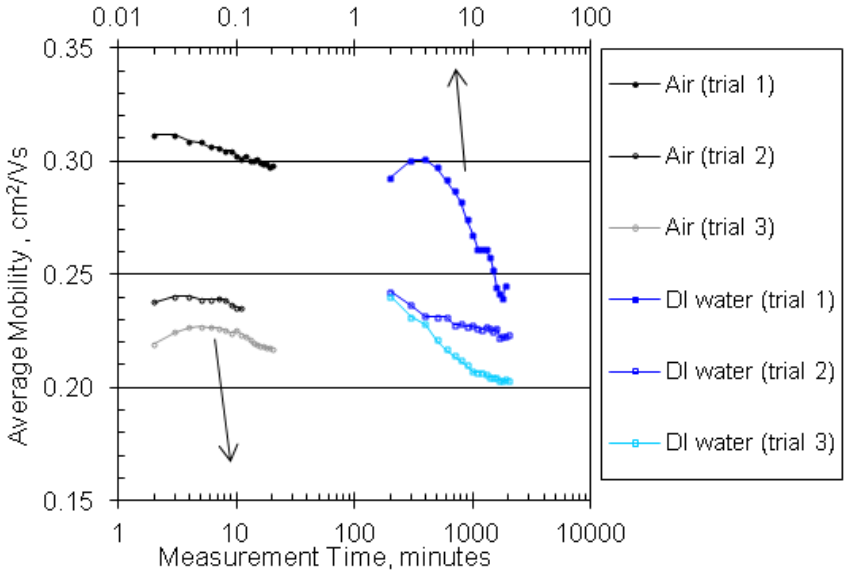

Figure 4-16 Average mobility evolution in microfluidics PTFT

The average mobility in air trial 1 was 0.303 cm^2/Vs. When the DI water was injected into the microfluidics channel on the top of the PTFT, then the average of the mobility in the first trial with DI water decreased to 0.27 cm^2/Vs. However, the reduction of the

mobility in DI water was only 10.9 % of original value, and remained virtually unchanged in following trails both with air and water in the microfluidics channel, as shown in figure 4-15. The water trap charge carriers and slightly decreases the mobility [65],[66]. In figure 4-16, the average mobility on the left is from the air trials; and the average mobility on the right is from the DI water trials. Both with and without DI water the mobility is between 0.31 cm^2/Vs and 0.20 cm^2/Vs , especially in trials 2 and 3, the mobility remains virtually unchanged. A similar result that water induced little decrease of mobility of PTFT has been reported in [53], where the long term operation of the 5,5'-bis-(7-dodecyl-9H-fluoren-2-yl)-2,2'-bithiophene (DDFTTF) OTFT directly exposed to DI water remains stable. The change of mobility and threshold voltage happens within minutes after the exposure of the TFT to water. Once the water in the organic semiconductor saturating, both the mobility and threshold voltage maintain stable values in the following ten thousands cyclic DI water measurements [53].

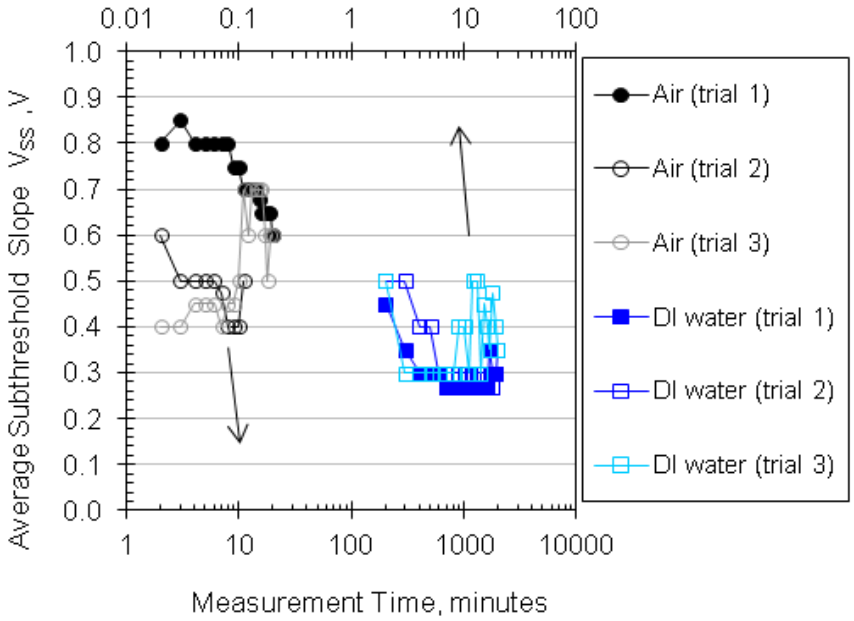

Figure 4-17 Evolution of the average subthreshold slope in the microfluidics PTFT transfer characteristics (linear and saturation regimes at V_D =-1V/-60V, respectively, gate bias voltage V_G =±20~-60V)

The average of subthreshold slope slightly deceases once the PTFTs exposing to DI water, shown in figure 4-17. The leakage current, figure 4-18, shows slightly decreasing with time, and DI water slightly deceases the off current comparing with air measurements. However, in the paper [24], water increases the off current of the P3HT PTFT, which is not observed here. The water at grain boundaries trap charge carriers [65] and decrease the conductivity of the polymer in off state, therefore, decreases the subthreshold slope and off current.

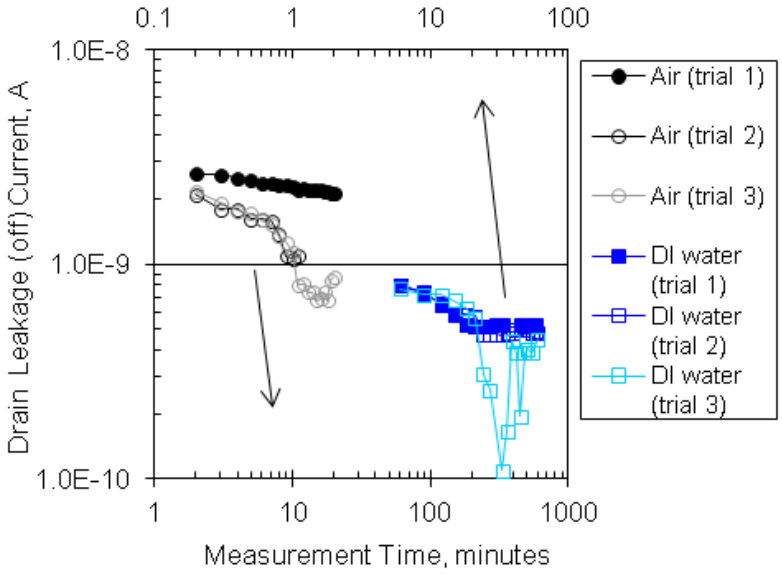

Figure 4-18 Off current evolution from the transfer characteristic in the saturation regime

4.3.2 Device with pH Solution in the microfluidics channel

The pH=1.5 solutions is the 12.39M HCL: DI water 1:10. The pH=10 buffer is from BDH Chemicals and contains Sodium Bicarbonate ~0.21 wt%, Sodium Carbonate~0.26 wt%, and DI water. The transfer characteristics of microfluidic PTFTs under different experiment conditions (air, DI water, pH=1.5 and 10 solution) are shown in figure 4-19. The pH=1.5 solution slightly increase PTFT's current at low gate bias, probably because the hydronium ions H_3O^+diffuse into the polymer and increase the current [53]. However, it decreases the drain current at high gate bias, probably because high ionic conduction in the acidic solution degrade the current. However, removing the acidic solution, the PTFT current at high gate bias recovered in the DI water measurements. The microfluidics

PTFT was left in air for two days and measured with DI water, air, pH=10 buffer solution in the microfluidics channel. The pH=10 buffer solution degraded the PTFT immediately, which probably because electrochemical damage of the organic thin film [53].

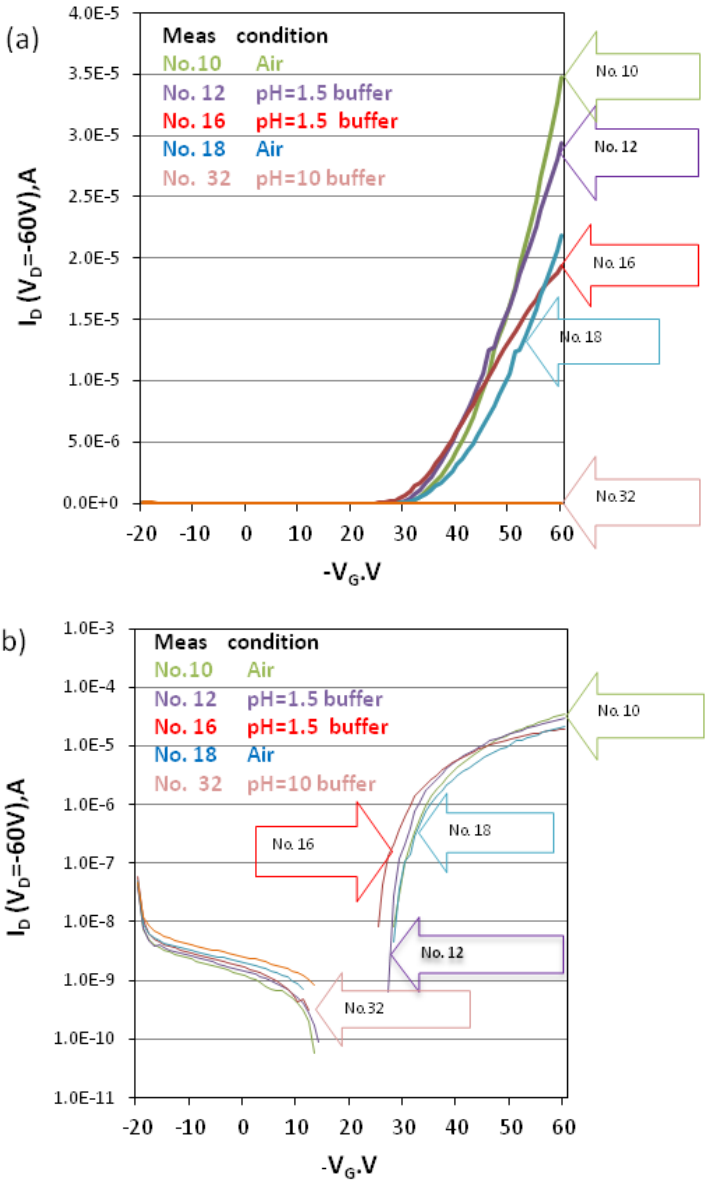

Figure 4-19 Transfer characteristics of the microfluidics PTFT in the saturation regime alternating in Air/ pH=1.5 and 10 buffer solutions.

The threshold voltage in DI water, as shown in figure 4-20, is slightly higher than in the air which was discussed in section 4.2.1. In the pH=1.5 acid solution measurements, the threshold voltage remains stable, probably because the diffused hydronium ions H_3O^+ compensate for the build-up charges owing to bias effect.

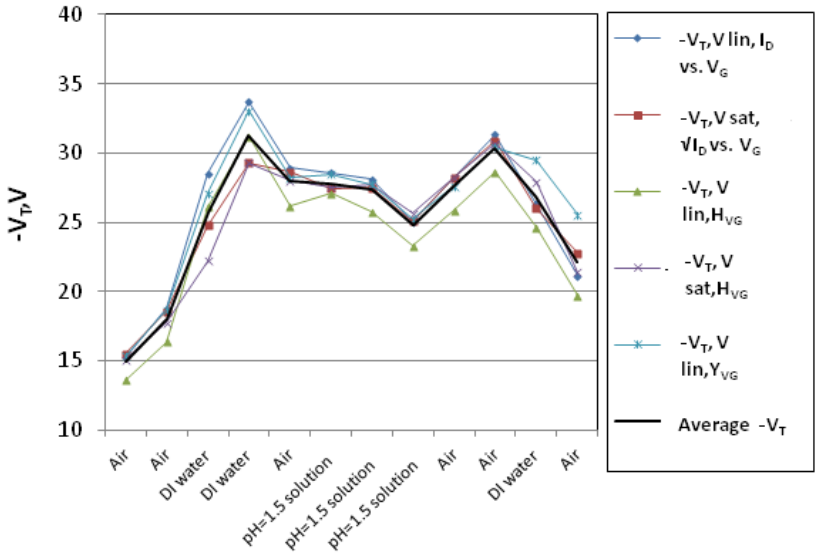

Figure 4-20 Threshold voltage evolution in the transfer characteristics (V_D=-1/-60V, V_G =±20~-60V) of the microfluidics PTFT

The changes of measurement conditions, such as alternating DI water and acid solution, increase the spread between the mobility values extracted from different characterization techniques, as shown in figure 4-21. However, the time seems reduces the spread, which also seen in the air/illumination measurements. The average of the mobility in pH=1.5 acid solution measurements increases comparing with the DI water measurements, probably because the diffused hydronium ions H_3O^+ in the polymer compensate for the

trapped charges in water. Again, the two days of storage of device did not decrease the mobility.

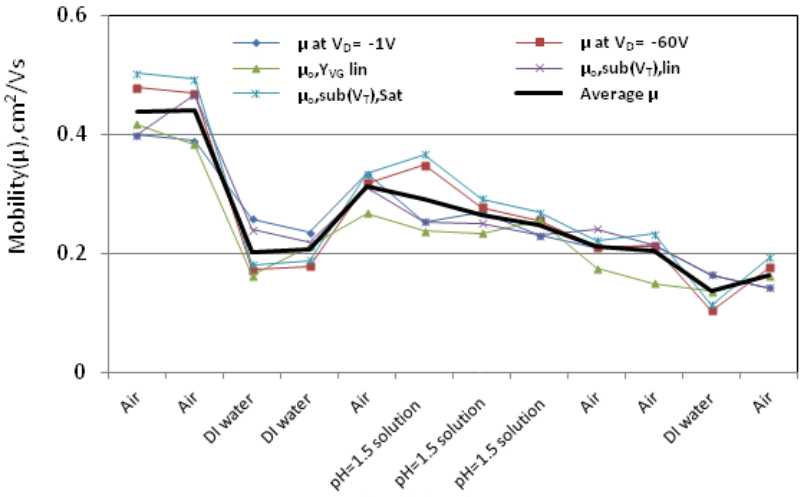

Figure 4-21 Mobility evolution in the transfer characteristic (V_D =-1/-60V, V_G =±20~-60V) of the microfluidics PTFT

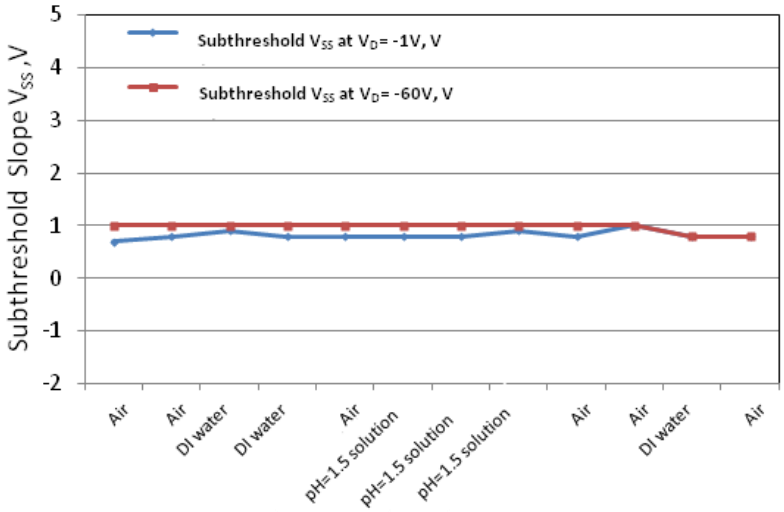

Figure 4-22 Subthreshold slope evolution of the transfer characteristic (linear and saturation regimes, V_D =-1V/-60V, V_G =±20~-60V) of the microfluidics PTFT

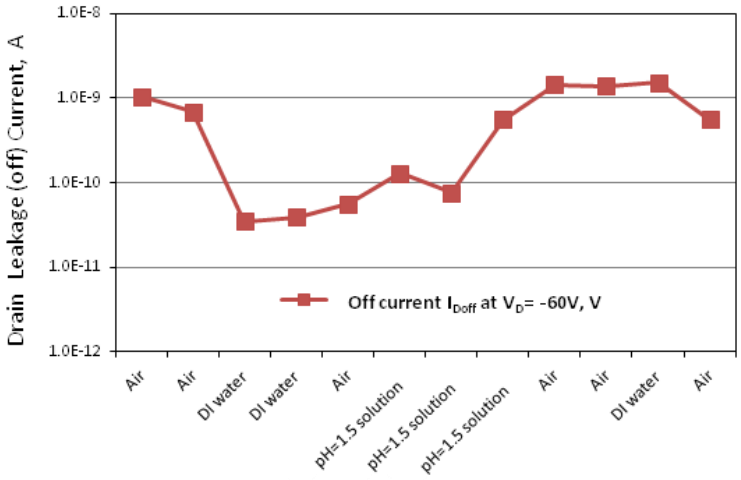

Figure 4-23 The off current evolution in the transfer characteristic for the saturation regime of the microfluidics PTFT

The subthreshold slopes V_{SS}, in figure 4-22, didn't show any dependence on neither the change of measurement condition, nor time. The off current of the microfluidics PTFT with liquid solution in the microfluidics channel shows lower values (DI water/acid solution in figure 4-23), which corresponds to the observation in section 4.2.1 and 4.2.2. Again, the two days storage did not affect the off current, showing an independence of time.

4.3.3 Device with salt solution in the microfluidics channel

The KCl and NaCl (from Caledon Laboratory Chemicals) was dissolved in DI water and injected into the microfluidic channel of the microfluidics PTFT, the 0.01M KCl and NaCl solutions didn't damage the device, where Bao et al. reported that 1M NaCl solution measurements shows negligible difference between water measurements [53].

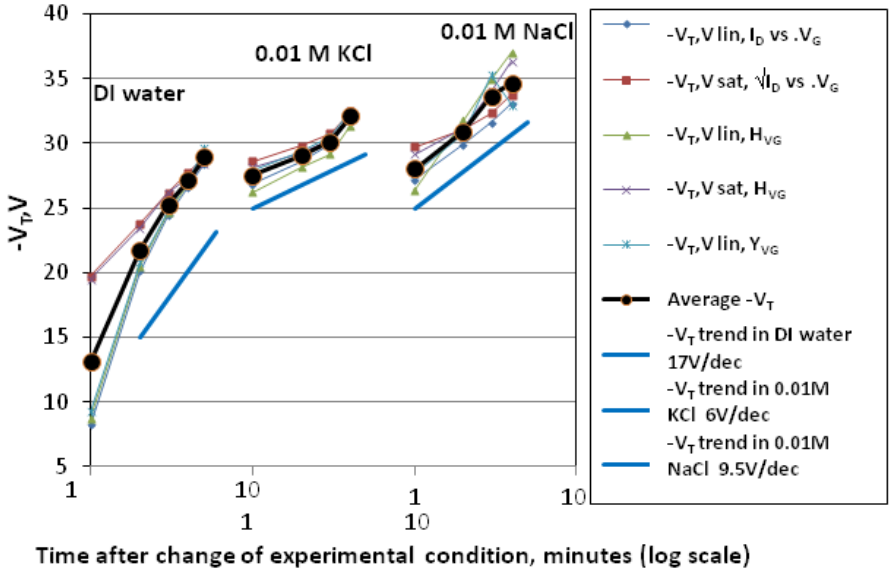

Figure 4-24 Threshold voltage evolution in the transfer characteristics (V_D =-1/-60V, V_G =±20~-60V) of the microfluidics PTFT with DI and salt water in the microfluidic channel

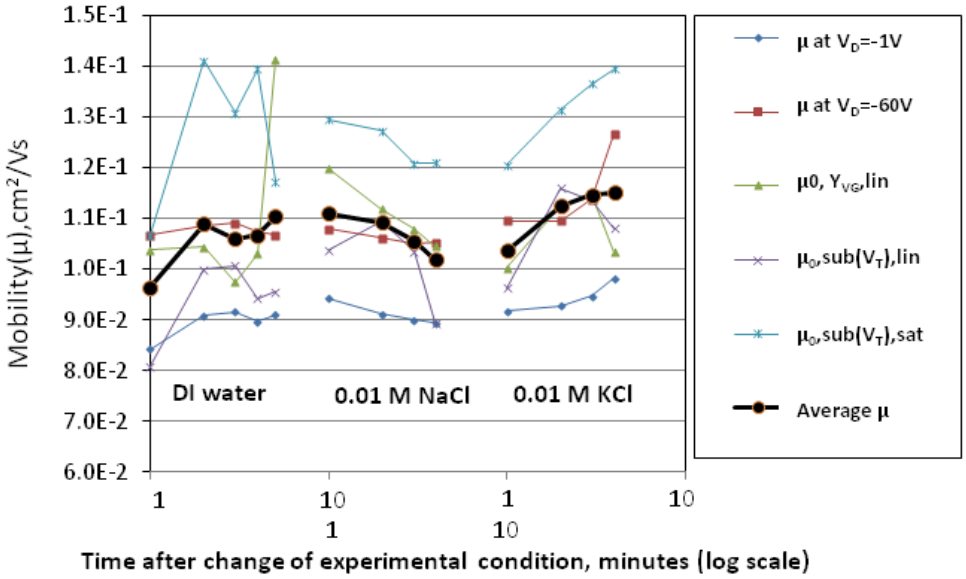

Figure 4-25 Mobility evolution in the transfer characteristics (V_D =-1/-60V, V_G =±20~-60V) of the microfluidic PTFT with DI and salt water in the microfluidic channel

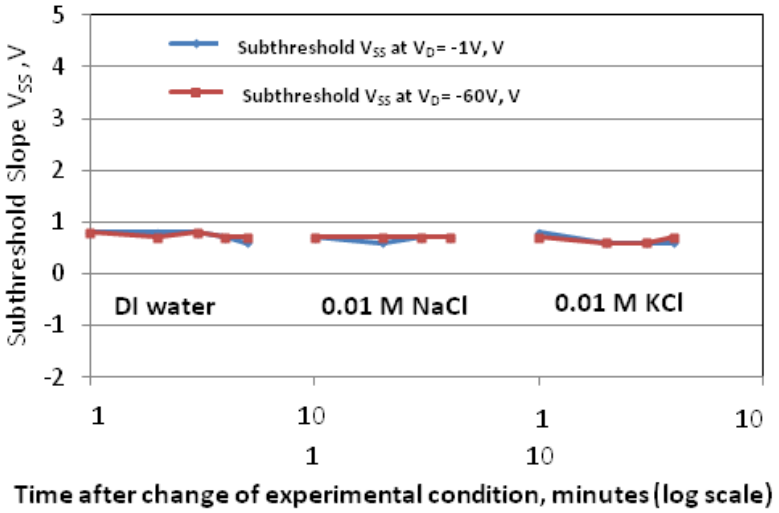

Figure 4-26 The subthreshold slope evolution in the transfer characteristics (linear and saturation regimes, V_D=-1V/-60V, V_G= ±20~-60V) of the microfluidic PTFT with DI and salt water in the microfluidic channel

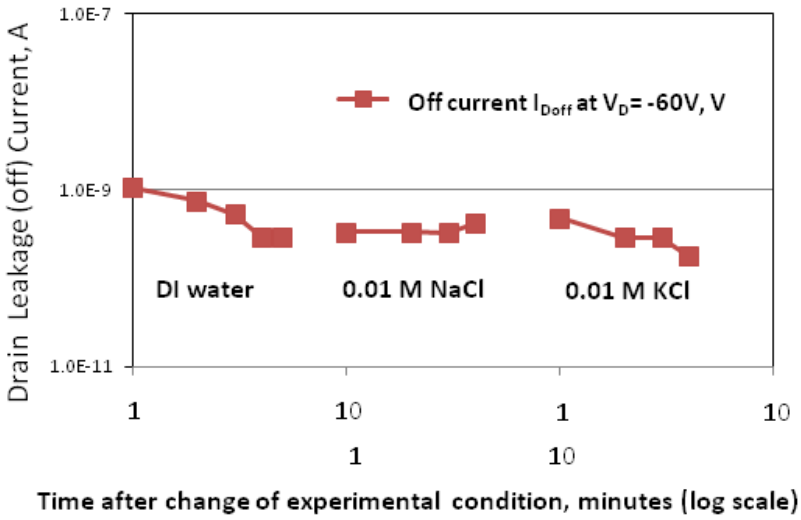

Figure 4-27 The off current evolution in the transfer characteristics for the saturation regime (V_D=-60V) of the microfluidics PTFT with DI and salt water in the microfluidic channel

The threshold voltage increases nearly logarithmically with the time, as seen in figure 4-24. The logarithmic variation of the threshold voltage with time is with a slope of ~17V/dec in DI water. The slope changed to 6V/dec in KCl and to 9.5V/dec in NaCl solutions. Salt water seems decreasing the slope of the time variation of the threshold voltage. However, the salt water does not affect the mobility, subthreshold slope and the leakage current of the microfluidics PTFT, as seen in figures 4-25, 4-26 and 4-27.

Chapter 5 Summary and Conclusion

The potential of low-cost, high-throughput fabrication and sensing property of printed polymeric thin film transistor drives the research on the PTFTs. However, the poor stability of the PTFT in inert, room and other (e.g., wet) environments causes difficulties in the commercializing of the organic electronics. Further research for understanding of the physical and chemical mechanisms in the PTFTs is still needed. Therefore, the environmental study of the PTFTs and the integration of the PTFT with microfluidics, which allows for studying the specific response of the organic semiconductors to the different solutions, are important research topics of the PTFTs.

5.1 Summary of PTFTs in different environments

The DKPP-βT polymeric thin film shows high mobility (~0.3cm^2/Vs). In the air and dark measurement, the threshold voltage continuously shifts, which was also reported in [49],[50],[47], following a logarithmic law as a function of the time. The increase of threshold voltage is due to the charge build-up within the semiconductor material [51] or chemical mechanism, since the recovery of the threshold voltage take days [49],[50].The mobility remains unchanged, which was also reported in [47],[26] as well as the subthreshold voltage and off current remain stable in time. Under light illumination, the light shifts the initial value of the threshold voltage towards more positive value. Because the photons are absorbed in the polymer [62] and release the trapped charge carriers [36]. The released charge carriers can move under electrical field, and reduce the threshold

voltage. However, in the consecutive same condition measurements, the charge carriers are trapped in the localized states and threshold voltage is increased. However, the mobility is unaffected by light, which is also reported in [25].The subthreshold slope senses the light, but no linear dependence observed. However, the off current varies proportionally with the light intensity. Because the increase of carrier density raises the conductivity of polymer, hereby increase the off current and subthreshold slope. The contact resistance (at $(-V_G) > (-V_T)$) extracted by the transmission line model (TLM) using PTFTs with different channel lengths compensating for threshold voltage and mobility enhancement factor, shows constant values. Therefore, the contact resistance of bottom-gated top-contact DKPP-βT polymeric thin film transistor does not depend on gate bias, neither on illumination.

The microfluidics PTFTs with air and DI water in the microfluidic channel measurements show that the threshold voltage in both measurements follows a logarithmic law function of time and the slope of the logarithmic law changes only in the beginning. The mobility slightly decreases in the beginning of exposing to DI water, which is also reported in [53]. The water molecules probably go through the active layer once exposing it to the device. The water molecules locate at grain boundaries and trap charge carriers, resulting in the changes of threshold voltage and mobility in the beginning. The mobility and the threshold voltage remain stable after that [53]. The subthreshold slope slightly deceases once the PTFTs exposing to DI water. The off current in DI water slightly decreases comparing with air measurement, which shows opposite result in the paper [24] where the DI water increases the off current.

In the pH=1.5 measurements, the threshold voltage remains stable and mobility slightly increased compared with water measurements, probably because the diffused hydronium ions H_3O^+ compensate for the trapped charge and increase the mobility. The subthreshold slope as well as the off current virtually does not change comparing with the DI water measurement. However, the pH=10 buffer solution damages the device immediately after exposing it to the device, which is probably because of an electrochemical damage to the organic thin film [53]. Measurements of the microfluidics PTFT with salt water (0.01M KCl and 0.01M NaCl) show results similar to the measurements in DI water.

Chapter 6 Contributions and Future Work

6.1 Contributions

The novel organic semiconductor, DKPP-βT based PTFT shows high mobility (~0.3cm^2/Vs). Therefore, the stability study is the next step in DKPP-βT PTFT research and crucial for its application. Based on the discussion in the previous chapter, the contribution in this work can be divided into two parts. First is the operation stability study of DKPP-βT PTFT under different intensities of illumination. Second, the unique microfluidics PTFT was fabricated and its sensing property with DI water, acid, base and salt solution were investigated.

6.1.1 PTFTs under illumination

Different extraction techniques introduced in section 2.2 were used to obtain threshold voltage V_T, mobility μ, subthreshold slope V_{SS}, and off current I_{Doff}. The parameter values extracted using different techniques vary, but the average values follow certain trends. The threshold voltage V_T falls more into a logarithmic law function of the time comparing with the power-law function [47],[49],[50], and exponential law function [40] of time in the literature. The light shifts the initial value of the threshold voltage towards more positive value with a linear relationship as 10~ 12 V/ (mW/cm^2). The mobility is unaffected neither by time (also reported in [25]) nor by light. However, the off current changes proportional with light. Also, the threshold voltage and mobility enhancement factor compensated TLM method demonstrates that the contact resistance (at $(-V_G) >$

$(-V_T)$) of bottom-gated top-contact DKPP-βT PTFT is constant and does not vary on gate bias nor on illumination. The ohmic contact resistance is desired, while very often in the literature undesirable bias-dependent contacts in organic thin film transistors are reported [50],[64].

6.1.2 Microfluidics PTFTs

The potential use of PTFT as biosensor needs the active part working under liquid medium. The novel microfluidics PTFT allows only the semiconductor channel exposed to liquid analytes and enables studying the sensing property of the DKPP-βT PTFT. The threshold voltage V_T evolution in the DI water measurements also follows logarithmic function of the time. The slope of the logarithmic function in DI water is slightly steeper than it in air. The mobility only decreases in the beginning of exposing to DI water, which is also reported in literature [53]. The off current in DI water slightly decreases comparing with air measurement, while in the paper [24] DI water increases the off current. In the acid solution measurement at low gate bias, the threshold voltage remains stable and mobility slightly increased compared with water measurements. Also, the threshold voltage, mobility in salt water measurements and the subthreshold slope, off current in both acid solution and salt water measurements show virtually similar results to DI water measurements. While the base solution damages the device immediately. The stable performance of DKPP-βT PTFTs with DI water and low-contraction salt water in the microchannel makes it promising as a biosensor.

6.2 Future Work

6.2.1 Fabrication

The PDMS microfluidic channel was attached to the PTFT manually under microscope. Therefore, the dimension of microfluidics PTFT is 6000μm and 500μm for width and length respectively, which is huge comparing with transistors in circuits and material consuming. Also, for the protection of source and drain electrodes from exposing to liquid in the channel, the microfluidic channel width is only 2/5 of the distance between drain and source, as shown in figure 4-11 (a). The integration or fabrication method needs to be improved to increase the ratio of the microfluidic channel width and the distance between drain and source and raise sensitivity.

6.2.2 Experiment setup

In early days, most PTFTs are measured in vacuum to protect from the contaminations in air. Since the DKPP-βT PTFT shows good stability and the disposable biosensors need active part expose to analytes in air, the measurements in this thesis are in air. However, the vacuum measurement is still needed to test the PTFT performance without oxygen, hydrogen or other gases in air. From the vacuum measurement, the significance of PTFT encapsulation and the physical and chemical mechanisms of PTFT can be studied.

The measurements of microfluidics PTFT with liquid in the microchannel were implemented by manually pushing liquid or air into the microchannel. During the measurements, the liquid was not flowing in the microchannel. Instead, it can be designed with a syringe pump that pushes the liquid flowing through the microchannel in

a constant velocity. Using such experiment setup, the microfluidic PTFT sensing property to certain liquid at various flowing velocity can be obtained.

6.2.3 Bio-sensor

The microfluidics PTFT fabricated in this thesis can be further used as bio-sensor. Several groups has fabricated PTFT bio-sensors, including sensing lactic acid [52], glucose [52],[53], cysteine [53] etc. However, none of them had the microfluidics channel across entire conduction channel of PTFT. The microfluidics PTFT in this thesis is proper to test the sensing property of glucose, lactic acid, protein etc.. Also, the PTFT can be used as a DNA sensor, because the phosphate groups on the backbone of DNA can attract electrons and shift the PTFT threshold voltage (p-type) towards more positive value [23].

References

[1] G. Inzelt, Conducting Polymers: A New Era in Electrochemistry. Berlin Heidelberg: Springer-Verlag, 2012.

[2] H. Letheby, "XXIX.—On the production of a blue substance by the electrolysis of sulphate of aniline," Journal of the Chemical Society, vol. 15, pp. 161-163, 1862.

[3] R. McNeill, R. Siudak, J. Wardlaw and D. Weiss, "Electronic conduction in polymers. I. The chemical structure of polypyrrole," Aust. J. Chem., vol. 16, pp. 1056-1075, 1963.

[4] B. Bolto, R. McNeill and D. Weiss, "Electronic conduction in polymers. III. Electronic properties of polypyrrole," Aust. J. Chem., vol. 16, pp. 1090-1103, 1963.

[5] C. Chiang, C. Fincher Jr, Y. Park, A. Heeger, H. Shirakawa, E. Louis, S. Gau and A. G. MacDiarmid, "Electrical conductivity in doped polyacetylene," Phys. Rev. Lett., vol. 39, pp. 1098-1101, 1977.

[6] H. Shirakawa, E. J. Louis, A. G. MacDiarmid, C. K. Chiang and A. J. Heeger, "Synthesis of electrically conducting organic polymers: halogen derivatives of polyacetylene,(CH)x," J.Chem.Soc., Chem.Commun., pp. 578-580, 1977.

[7] C. Chiang, Y. Park, A. Heeger, H. Shirakawa, E. Louis and A. G. MacDiarmid, "Conducting polymers: halogen doped polyacetylene," J. Chem. Phys., vol. 69, pp. 5098, 1978.

[8] Nobelprize.org. The nobel prize in chemistry 2000. [Online]. 2012(10/23), 2012. Available: http://www.nobelprize.org/nobel_prizes/chemistry/laureates/2000/.

[9] H. Koezuka, A. Tsumura and T. Ando, "Field-effect transistor with polythiophene thin film," Synth Met, vol. 18, pp. 699-704, 1987.

[10] Samsung Inc. Samsung galaxy S III™. [Online]. 2012(11/25), 2012. Available: http://www.samsung.com/ca/consumer/mobile/mobile-phones/smartphones/SGH-I747MBABMC.

[11] Sony Electronics Inc. TRIMASTER EL™ series OLED monitors. [Online]. 2012(10/22), 2012. Available: http://pro.sony.com/bbsc/ssr/cat-monitors/cat-oledmonitors/.

[12] S. R. Forrest, "The path to ubiquitous and low-cost organic electronic appliances on plastic," Nature, vol. 428, pp. 911-918, 2004.

[13] J. T. Mabeck and G. G. Malliaras, "Chemical and biological sensors based on organic thin-film transistors," Analytical and Bioanalytical Chemistry, vol. 384, pp. 343-353, 2006.

[14] H. Laurs and G. Heiland, "Electrical and optical properties of phthalocyanine films," Thin Solid Films, vol. 149, pp. 129-142, 1987.

[15] M. Bouvet, G. Guillaud, A. Leroy, A. Maillard, S. Spirkovitch and F. G. Tournilhac, "Phthalocyanine-based field-effect transistor as ozone sensor," Sensors Actuators B: Chem., vol. 73, pp. 63-70, 2001.

[16] L. Torsi, A. Dodabalapur, L. Sabbatini and P. G. Zambonin, "Multi-parameter gas sensors based on organic thin-film-transistors," Sensors Actuators B: Chem., vol. 67, pp. 312-316, 2000.

[17] Z. T. Zhu, J. T. Mason, R. Dieckmann and G. G. Malliaras, "Humidity sensors based on pentacene thin-film transistors," Appl. Phys. Lett., vol. 81, pp. 4643-4645, 2002.

[18] D. Li, E. J. Borkent, R. Nortrup, H. Moon, H. Katz and Z. Bao, "Humidity effect on electrical performance of organic thin-film transistors," Appl. Phys. Lett., vol. 86, pp. 042105-042105-3, 2005.

[19] L. Torsi, A. Dodabalapur, N. Cioffi, L. Sabbatini and P. Zambonin, "NTCDA organic thin-film-transistor as humidity sensor: weaknesses and strengths," Sensors Actuators B: Chem., vol. 77, pp. 7-11, 2001.

[20] B. Crone, A. Dodabalapur, A. Gelperin, L. Torsi, H. Katz, A. Lovinger and Z. Bao, "Electronic sensing of vapors with organic transistors," Appl. Phys. Lett., vol. 78, pp. 2229-2231, 2001.

[21] L. Torsi, M. Tanese, N. Cioffi, M. Gallazzi, L. Sabbatini, P. Zambonin, G. Raos, S. Meille and M. Giangregorio, "Side-chain role in chemically sensing conducting polymer field-effect transistors," The Journal of Physical Chemistry B, vol. 107, pp. 7589-7594, 2003.

[22] J. Y. Wang, W. Chen, A. H. Liu, G. Lu, G. Zhang, J. H. Zhang and B. Yang, "Controlled fabrication of cross-linked nanoparticles/polymer composite thin films through the combined use of surface-initiated atom transfer radical polymerization and gas/solid reaction," J. Am. Chem. Soc., vol. 124, pp. 13358-13359, 2002.

[23] Q. Zhang and V. Subramanian, "DNA hybridization detection with organic thin film transistors: Toward fast and disposable DNA microarray chips," Biosensors and Bioelectronics, vol. 22, pp. 3182-3187, 2007.

[24] C. H. Chang, M. F. Chen and C. H. Chien, "An Investigation of Transient Effects in Poly (3-hexylthiophenes) Based Thin Film Transistors Caused by Oxygen and Water Molecules," J. Electrochem. Soc., vol. 158, pp. H854, 2011.

[25] A. Völkel, R. Street and D. Knipp, "Carrier transport and density of state distributions in pentacene transistors," Physical Review B, vol. 66, pp. 195336, 2002.

[26] J. B. Chang and V. Subramanian, "Effect of active layer thickness on bias stress effect in pentacene thin-film transistors," Appl. Phys. Lett., vol. 88, pp. 233513, 2006.

[27] B. A. Mattis and V. Subramanian, "Enabling technologies for organic memories," Ph.D. dissertation, Dept. EECS., University of California at Berkeley, Berkeley, CA, 2006.

[28] F. Garnier, R. Hajlaoui, A. Yassar and P. Srivastava, "All-polymer field-effect transistor realized by printing techniques." Science, vol. 265, pp. 1684, 1994.

[29] G. Horowitz, "Organic thin film transistors: From theory to real devices," J. Mater. Res., vol. 19, pp. 1946-1962, 2004.

[30] Q. Zhang, "OTFT-based DNA detection system," Ph.D. dissertation, Dept. EECS., University of California at Berkeley, Berkeley, CA, 2007.

[31] J. A. Rogers, Z. Bao, A. Makhija and P. Braun, "Printing process suitable for reel-to-reel production of high-performance organic transistors and circuits," Adv Mater, vol. 11, pp. 741-745, 1999.

[32] Fujifilm Co. Materials printer & cartridges DMP-2831 & DMC-11601/11610 datasheet. [Online]. 2012(09/30), 2011. Available: http://www.fujifilmusa.com/shared/bin/DMP-2831_Datasheet.pdf.

[33] H. P. Le, "Progress and trends in ink-jet printing technology," The Journal of Imaging Science and Technology, vol. 42, pp. 49-62, 1998.

[34] I. Kymissis, C. Dimitrakopoulos and S. Purushothaman, "High-performance bottom electrode organic thin-film transistors," IEEE Transactions on Electron Devices, vol. 48, pp. 1060-1064, 2001.

[35] M. J. Deen, M. H. Kazemeini and S. Holdcroft, "Contact effects and extraction of intrinsic parameters in poly (3-alkylthiophene) thin film field-effect transistors," J. Appl. Phys., vol. 103, pp. 124509-124509-7, 2008.

[36] Z. Bao and J. Locklin, Organic Field-Effect Transistors. Boca Raton, FL: CRC Press, 2007.

[37] IBchem.com. Bonding(hl)- hybridisation. [Online]. 2012(10/25), 2004. Available: http://ibchem.com/IB/ibnotes/full/bon_htm/14.2.htm.

[38] O. Marinov, M. Deen and R. Datars, "Compact modeling of charge carrier mobility in organic thin-film transistors," J. Appl. Phys., vol. 106, pp. 064501-064501-13, 2009.

[39] O. Marinov, M. J. Deen, U. Zschieschang and H. Klauk, "Organic thin-film transistors: Part I—Compact DC modeling," IEEE Transactions on Electron Devices, vol. 56, pp. 2952-2961, 2009.

[40] H. Gomes, P. Stallinga, F. Dinelli, M. Murgia, F. Biscarini, D. De Leeuw, T. Muck, J. Geurts, L. Molenkamp and V. Wagner, "Bias-induced threshold voltages shifts in thin-film organic transistors," Appl. Phys. Lett., vol. 84, pp. 3184, 2004.

[41] A. Cerdeira, M. Estrada, R. Garcıa, A. Ortiz-Conde and F. Garcıa Sánchez, "New procedure for the extraction of basic a-Si: H TFT model parameters in the linear and saturation regions," Solid-State Electronics, vol. 45, pp. 1077-1080, 2001.

[42] M. J. Deen, O. Marinov, U. Zschieschang and H. Klauk, "Organic Thin-Film Transistors: Part II—Parameter Extraction," IEEE Transactions on Electron Devices, vol. 56, pp. 2962-2968, 2009.

[43] G. Ghibaudo, "New method for the extraction of MOSFET parameters," Electron. Lett., vol. 24, pp. 543-545, 1988.

[44] Y. Xu, T. Minari, K. Tsukagoshi, R. Gwoziecki, R. Coppard, F. Balestra, J. Chroboczek and G. Ghibaudo, "Extraction of low-frequency noise in contact resistance of organic field-effect transistors," Appl. Phys. Lett., vol. 97, pp. 033503-033503-3, 2010.

[45] G. Reeves and H. Harrison, "Obtaining the specific contact resistance from transmission line model measurements," IEEEE Lectron Device Letters, vol. 3, pp. 111-113, 1982.

[46] Y. Qiu, Y. Hu, G. Dong, L. Wang, J. Xie and Y. Ma, "H2O effect on the stability of organic thin-film field-effect transistors," Appl. Phys. Lett., vol. 83, pp. 1644, 2003.

[47] A. Salleo, F. Endicott and R. Street, "Reversible and irreversible trapping at room temperature in poly (thiophene) thin-film transistors," Appl. Phys. Lett., vol. 86, pp. 263505, 2005.

[48] M. J. Deen and M. H. Kazemeini, "Photosensitive polymer thin-film FETs based on poly (3-octylthiophene)," Proc IEEE, vol. 93, pp. 1312-1320, 2005.

[49] A. Salleo, M. Chabinyc, M. Yang and R. Street, "Polymer thin-film transistors with chemically modified dielectric interfaces," Appl. Phys. Lett., vol. 81, pp. 4383, 2002.

[50] R. J. Chesterfield, J. C. McKeen, C. R. Newman, C. D. Frisbie, P. C. Ewbank, K. R. Mann and L. L. Miller, "Variable temperature film and contact resistance measurements on operating n-channel organic thin film transistors," J. Appl. Phys., vol. 95, pp. 6396, 2004.

[51] D. Knipp, R. Street, A. Völkel and J. Ho, "Pentacene thin film transistors on inorganic dielectrics: Morphology, structural properties, and electronic transport," J. Appl. Phys., vol. 93, pp. 347, 2003.

[52] T. Someya, A. Dodabalapur, A. Gelperin, H. E. Katz and Z. Bao, "Integration and response of organic electronics with aqueous microfluidics," Langmuir, vol. 18, pp. 5299-5302, 2002.

[53] M. E. Roberts, S. C. B. Mannsfeld, N. Queraltó, C. Reese, J. Locklin, W. Knoll and Z. Bao, "Water-stable organic transistors and their application in chemical and biological sensors," Proceedings of the National Academy of Sciences, vol. 105, pp. 12134, 2008.

[54] H. Sirringhaus, N. Tessler and R. H. Friend, "Integrated optoelectronic devices based on conjugated polymers," Science, vol. 280, pp. 1741-1744, 1998.

[55] B. S. Ong, Y. Wu, P. Liu and S. Gardner, "High-performance semiconducting polythiophenes for organic thin-film transistors," J. Am. Chem. Soc., vol. 126, pp. 3378-3379, 2004.

[56] Y. Li, P. Sonar, S. P. Singh, M. S. Soh, M. van Meurs and J. Tan, "Annealing-Free High-Mobility Diketopyrrolopyrrole− Quaterthiophene Copolymer for Solution-Processed Organic Thin Film Transistors," J. Am. Chem. Soc., vol. 133, pp. 2198-2204, 2011.

[57] X. Zhang, L. J. Richter, D. M. DeLongchamp, R. J. Kline, M. R. Hammond, I. McCulloch, M. Heeney, R. S. Ashraf, J. N. Smith and T. D. Anthopoulos, "Molecular packing of high-mobility diketo pyrrolo-pyrrole polymer semiconductors with branched alkyl side chains," J. Am. Chem. Soc., vol. 133, pp. 15073-15084, 2011.

[58] Y. Li, P. Sonar, S. P. Singh, M. S. Soh, M. van Meurs and J. Tan, "Annealing-Free High-Mobility Diketopyrrolopyrrole− Quaterthiophene Copolymer for Solution-Processed Organic Thin Film Transistors," J. Am. Chem. Soc., 2011.

[59] M. Jin, X. Feng, J. Xi, J. Zhai, K. Cho, L. Feng and L. Jiang, "Super- Hydrophobic PDMS Surface with Ultra- Low Adhesive Force," Macromolecular Rapid Communications, vol. 26, pp. 1805-1809, 2005.

[60] M. C. Hamilton, S. Martin and J. Kanicki, "Thin-film organic polymer phototransistors," IEEE Transactions on Electron Devices, vol. 51, pp. 877-885, 2004.

[61] M. C. Hamilton and J. Kanicki, "Organic polymer thin-film transistor photosensors," IEEE Journal of Selected Topics in Quantum Electronics, vol. 10, pp. 840-848, 2004.

[62] A. M. Fox and M. Fox, Optical Properties of Solids. New York: Oxford University Press, 2001.

[63] K. Narayan and N. Kumar, "Light responsive polymer field-effect transistor," Appl. Phys. Lett., vol. 79, pp. 1891-1893, 2001.

[64] D. Gundlach, L. Zhou, J. Nichols, T. Jackson, P. Necliudov and M. Shur, "An experimental study of contact effects in organic thin film transistors," J. Appl. Phys., vol. 100, pp. 024509-024509-13, 2006.

[65] D. Li, E. J. Borkent, R. Nortrup, H. Moon, H. Katz and Z. Bao, "Humidity effect on electrical performance of organic thin-film transistors," Appl. Phys. Lett., vol. 86, pp. 042105-042105-3, 2005.

[66] T. Jung, A. Dodabalapur, R. Wenz and S. Mohapatra, "Moisture induced surface polarization in a poly (4-vinyl phenol) dielectric in an organic thin-film transistor," Appl. Phys. Lett., vol. 87, pp. 182109-182109-3, 2005.